R. & M. No. 2595
(9408, 11,163)
A.R.C. Technical Report

MINISTRY OF SUPPLY

AERONAUTICAL RESEARCH COUNCIL
REPORTS AND MEMORANDA

Tests of Model Propellers in the High Speed Tunnel Thrust and Torque Measurements on a 2-Blade, 6 per cent. Thick, Clark Y Section Propeller

By

G. S. Hislop, Ph.D., B.Sc., A.R.T.C., A.M.I.Mech.E., A.F.R.Ae.S.
and J. Caldwell, B.Sc., Wh.Sc., A.M.I.Mech.E., A.F.R.Ae.S.

With an Appendix by
M. Jones, B.Sc.

LONDON: HIS MAJESTY'S STATIONERY OFFICE
1951
PRICE 11s 6d NET

Tests of Model Propellers in the High Speed Tunnel Thrust and Torque Measurements on a 2-Blade, 6 per cent. thick, Clark Y Section Propeller

By

G. S. Hislop, Ph.D., B.Sc., A.R.T.C., A.M.I.Mech.E., A.F.R.Ae.S.
and J. Caldwell, B.Sc., Wh.Sc., A.M.I.Mech.E., A.F.R.Ae.S.

with an Appendix by

M. Jones, B.Sc.

Communicated by the Principal Director of Scientific Research (Air), Ministry of Supply

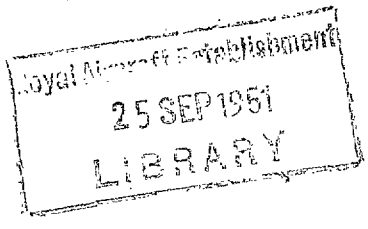

Reports and Memoranda No. 2595*

November, 1945

Summary.—Reason for Investigation.—High-speed wind tunnel tests of various model propellers were required as part of a general research programme dealing with propellers for high-speed aircraft.

Range of Investigation.—A two-blade 4 ft 6 in diameter Clark Y section propeller of 6 per cent. thickness ratio and 7 per cent. total solidity was tested at three fixed blade angles over a range of forward Mach numbers up to 0·8 and rates of advance up to $J = 4$. In addition, the forward Reynolds number based on 1 ft. chord, was varied from 1 million to 4 millions at one blade angle, the forward Mach number being held constant at 0·3.

Conclusions.—(i) The experimental technique employed for measurement of overall thrust and torque of model propellers in the Royal Aircraft Establishment High Speed Tunnel was proved successful and capable of yielding reasonably consistent results.

(ii) No appreciable scale effect was present on the tests made at low Mach number, but this does not necessarily hold at high Mach numbers, for which condition no evidence is available.

(iii) The variation of thrust and torque coefficients and propulsive efficiency with increasing Mach number at constant rates of advance show no serious departure from the variations to be expected from such a blade section operating at high Mach numbers.

(iv) A maximum efficiency of 0·9 was attained with this propeller at low forward speeds and tip Mach numbers. With increase in Mach number the efficiency fell slowly but steadily until some critical Mach number was reached when the rate of decrease became serious. The critical tip Mach number varied between 0·9 and 1·2 depending upon the operating conditions. At a forward Mach number of 0·7 and upwards the rate of decrease in efficiency became large, though the maximum efficiency at $M = 0·7$ was still quite high at 0·76. It might be possible to reduce this rate of decrease at a given Mach number by operating at still greater blade settings.

* R.A.E. Report Aero. 2096—received 7th February, 1948.
R.A.E. Report Aero. 2096a—received 21st January, 1948.

1. *Introduction.*—1.1. The necessity for testing representative modern propellers and typical propeller aerofoils at conditions corresponding to the speeds and rates of advance obtaining on present high-speed aircraft was recognised some considerable time ago. Accordingly a comprehensive research programme was drawn up involving (i) full-scale flight tests, (ii) wind-tunnel experiments on aerofoils suitable for high-speed propeller blades, and (iii) thrust and torque measurements on model propellers in various wind tunnels.

This report deals with the methods used in and results obtained from the initial series of tests in the Royal Aircraft Establishment High Speed Tunnel under the third heading.

1.2. To drive the propellers designed for this part of the programme required an electric motor capable of delivering 200 b.h.p. over the range of 4,000 to 8,000 r.p.m. and yet small enough to be mounted, suitably faired, in the working section of the High Speed Tunnel without undue blockage.

Such a motor has been designed and made and results are given of the initial tests carried out using the first of a series of propellers designed for these experiments. The tests were of a preliminary nature to cover the probable limits of future tests and to give as much experience as possible on running technique and to assess the accuracy and consistency of the system of measurements employed. As the results were satisfactory they have been presented here, whilst the various corrections due to tunnel blockage, etc. have been given in some detail as similar corrections will be applicable to future tests.

1.3. Since the completion of this initial series of experiments the motor has been returned to the manufacturers for certain alterations designed to improve its efficiency and running capabilities.

2. *Apparatus and Methods.*—2.1.—*General.*—The basic scheme for measuring the thrust and torque of the model propellers is as follows :—

The motor is mounted on the wind-tunnel balance and the propeller thrust derived from readings of the drag balance. The torque is obtained from measurement of the electrical power input and the motor running conditions, in conjunction with data from previous calibration tests.

Fig. 1 shows the arrangement of the motor and propeller in the working section of the tunnel.

2.2. *Propeller Motor.*—This is a squirrel cage induction motor, designed and built by Messrs. Metropolitan Vickers Electrical Co. Ltd., Manchester; it has a solid steel rotor (for mechanical stiffness reasons) and is rated at :—

Linear increase of power from 50 b.h.p. at 1,000 r.p.m. to 200 b.h.p. at 4,000 r.p.m.

Power constant at 200 b.h.p. from 4,000 to maximum r.p.m. of 8,000.

It is fed with a variable frequency, three phase, alternating current supply, the voltage being adjusted to give minimum electrical losses at each speed. The necessary variable frequency alternator and associated electrical machinery form part of the equipment of the R.A.E. 24-ft Tunnel, being used in that tunnel to drive a 1,500 h.p. propeller motor.

Cooling of the stator windings of the 200 h.p. motor is effected by pumping brine from the High Speed Tunnel supply through a jacket outside the windings. The various electrical and brine leads from the motor are led down a vertical strut behind the two oblique supporting struts and thence outside the tunnel (*see* Fig. 1). This rear strut is attached to the pitching moment arm of the balance (which arm is kept locked) and is not intended to carry any of the weight of the motor. The overall dimensions of the motor assembly, including the fairing and spinner are: length 120 in; maximum diameter 19·2 in.

The motor is calibrated by coupling it to an inductor type of dynamometer brake situated on a stand outside the wind-tunnel shell. The input to the motor is measured electrically whilst the torque exerted is transferred by suitable linkage to an Avery weighbridge. Rotational speed is measured by means of a Clerk-Maxwell bridge circuit, the necessary impulse for this system being supplied by a commutator on the non-driving end of the motor shaft. Basic details of this circuit are given in Fig. 2.

2.3. *Propeller.*—This propeller, the first of a series of 11 model propellers of 4 ft 6 in diameter designed for test by this apparatus, is designated ' No. 0 '. It has two steel blades of Clark Y section with a thickness/chord ratio of $0{\cdot}06$ from about $0{\cdot}4R$ to the tip, the solidity per blade being $0{\cdot}035$. Each blade of the propeller is set in the hub to the required blade angle and clamped tightly at this setting. Further details are given in Fig. 3, whilst Fig. 4 gives a general impression of the blades.

As a safety precaution the propeller was spun by the motor on a balancing stand prior to its first installation in the tunnel.

3. *Tests Made.*—3.1. *Without Propeller.*—Measurements of the drag of the motor assembly and struts were made in the absence of the propeller over a range of forward Mach numbers from $0{\cdot}2$ to $0{\cdot}8$ and also at a number of forward Reynolds numbers, based on 1-ft chord, between $0{\cdot}5 \times 10^6$ and 5×10^6. This experiment established the basic, or tare, drag of the installation from which was subtracted the observed drag balance readings with the propeller running to give a first approximation to the propeller thrust.

The results of the motor drag measurements are given in Fig. 5.

3.2. *With Propeller.*—The tests made with No. 0 propeller consisted of thrust and torque measurements at three different blade angles as measured at the $0{\cdot}7R$ station, viz. 40, 50 and 60 deg. (nominal values). At each blade angle the forward Mach number was varied in stages from a low to a high value, the maximum range covered being from $0{\cdot}2$ to $0{\cdot}8$ in the case of the 60 deg. setting. At each Mach number, a series of runs over the maximum range of J values was made, the higher limit being the windmilling condition whilst the lower limit was governed usually by propeller motor limitations.

All the above series of runs were made at a constant forward Reynolds number of 1×10^6. A fourth series of runs was made at the 60 deg. blade setting and a constant forward Mach number of $0{\cdot}3$ but varying the forward Reynolds number in four steps, viz. 1×10^6, 2×10^6, 3×10^6, 4×10^6, in order to obtain a check on any scale effect on thrust or torque coefficients.

The actual technique employed throughout was to run at fixed values of the ratio: Tunnel fan r.p.m./propeller r.p.s. (N/n) at each of the chosen values of forward Mach number. This corresponds roughly to a series of fixed values of J at each of the forward Mach numbers: curves at truly constant values of J were obtained afterwards by cross-plotting. To run at exactly constant values of J at each forward Mach number would have entailed complicated calculations for blockage, changes in temperature, etc., being made and allowed for in the course of a run.

A list of the experiments made is given in tabular form below :—

TABLE 1

Table of Experiments

Condition	Forward Mach number range	Forward Reynolds number	J Range	Pressures measured (*see* Appendix I)	Remarks
Empty tunnel	0·2 to 0·89 corrected	$\frac{1}{2} \times 10^6$ to 5×10^6	—	Far wall, near wall. Roof, floor.	Far and near walls give pressure coefficients sufficiently close to be regarded as the same. Floor coefficients unreliable due to presence of supports.
Motor alone	0·2 to 0·78 uncorrected	$\frac{1}{2} \times 10^6$ to 5×10^6	—	Far wall, near wall. Roof, floor. Motor fairing.	
Motor and propeller θ=39 deg. 35 min. at 0·7R	0·2 to 0·5 corrected	1×10^6 1×10^6 1×10^6	2·3 to 1·2	—	
Ditto. Repeat test	0·2 to 0·43 corrected	1×10^6 1×10^6 1×10^6	1·9 to 1·2	—	These tests were made two days after initial ones at this blade setting.
Motor and propeller θ=49 deg. 49 min. at 0·7R	0·2 to 0·78 corrected	1×10^6 1×10^6 1×10^6	3·0 to 1·6	—	
Motor and propeller θ=60 deg. 0 min. at 0·7R.	0·2 to 0·81 corrected	1×10^6 1×10^6 1×10^6	4·6 to 2·6	Far wall.	Pressure connections not made to correct datum.
Motor and propeller *θ=60 deg. approx. at 0·7R.	0·3 0·3 0·3 0·3 corrected	1×10^6 2×10^6 3×10^6 4×10^6	4·1 to 2·6	—	

4. *Correction and Reduction of Observed Results.*—4.1. *General.*—An outline only is given here of the various corrections employed, full details being given in appendices to the report. The observed values of drag and electrical input give respectively, when corrected, the thrust and torque of the propeller, whilst from the calculated value of blockage is derived the actual operating condition of the propeller. The principles underlying the derivation of these three basic corrections are dealt with separately as follows :—

4.2. *Correction to Tunnel Speed.*—The blockage calculations made in Appendix I aim at giving the speed of an infinite stream of free air which, flowing past a propeller mounted on the same body as in the tunnel tests, but without supporting struts, would give the same speed through the propeller disc as in the actual tunnel test. This condition means that at the same rotational speed the thrust and torque from the propeller in the tunnel is the same as would be obtained in a free stream.

The order of magnitude of the increment in tunnel velocity at the propeller disc is given in tabular form in Appendix I ; the greatest correction which was applied was 4·7 per cent. of the nominal tunnel velocity.

* It is suspected that a small change in blade angle took place between the last two test conditions, but this cannot be confirmed. It is best to assume that these two tests were not made at precisely the same setting.

4.3. *Corrections to Thrust.*—The observed drag balance reading with the propeller running is corrected to give thrust by the following method :—

$$\text{Thrust} = -\text{Observed drag balance reading} + \begin{cases} \text{(i) Tare drag of motor and struts.} \\ \text{(ii) Buoyancy correction due to pressure gradient.} \\ \text{(iii) Correction to (i) for decrease in general field speed caused by propeller blockage.} \\ \text{(iv) Increase of drag of struts due to increased speed in slipstream.} \end{cases}$$

Of these, (i) is a measured quantity, whilst the others are calculated quantities, most conveniently expressed as functions of a propeller thrust coefficient. Full details of these corrections are given in Appendix II, but it may be observed that the net correction under headings (ii), (iii), and (iv) above varies between -1 and -6 per cent. of the thrust over the range of forward Mach numbers up to $M = 0{\cdot}75$.

4.4. *Torque Determination.*—The underlying assumption in the determination of the motor b.h.p., and hence the torque, is that it can be obtained accurately from the measured electrical input by subtracting the motor losses at the appropriate operating conditions. The losses are obtained from separate calibration tests of the motor when coupled to a dynamometer. Normal electrical engineering methods of separating the losses into copper, iron, friction and windage losses are followed. Full details of the calibration technique and the results are given in Appendix III.

It may be noted here that the present tests are based on preliminary calibration of the motor in its original state, and as a result of experience a more comprehensive calibration is desirable. This will be done after the motor has been modified by the makers.

4.5. *Calculation of Coefficients, etc.*—From the calculated blockage figures and the observed tunnel conditions are derived corrected values of Mach number, air density, air temperature, and wind speed using the normal methods. The usual thrust and torque coefficients, propulsive efficiency, and tip Mach number, etc., were calculated from

$$\text{Thrust coefficient } K_T = \frac{T}{\rho n^2 D^4}$$

$$\text{Torque coefficient } K_Q = \frac{Q}{\rho n^2 D^5}$$

$$\text{Propulsive efficiency } \eta = \frac{J}{2\pi}\frac{K_T}{K_Q}$$

$$\text{Tip Mach number } M_{\text{tip}} = M\sqrt{\left[1 + \left(\frac{\pi}{J}\right)^2\right]}$$

5. *Results.*—The results are presented in the form of curves of thrust and torque coefficients and propulsive efficiency against J in Figs. 6, 7, 8, and 9; other curves derived from these are given in Figs. 10 to 21. It was considered that the results at forward Mach numbers greater than $0{\cdot}75$ were unreliable owing to the magnitude of the corrections involved (*see* Table 3, Appendix II). Consequently any such results have been omitted from this report.

The examination of the experimental results can be divided conveniently as follows.

5.1. *Tests at $\theta = 40$ deg.*—The results given in Figs. 6a, b, c, cover only a small range of forward Mach numbers but demonstrate that a reasonable degree of consistency and ability to repeat can be obtained from the experimental technique employed.

5.2. *Tests at Various Reynolds Number.*—Fig. 7 shows that the scale effect on the experimental results is negligible over a range of forward Reynolds numbers of 1×10^6 to 4×10^6 (based on 1-ft chord), for low Mach numbers at least. This range of forward Reynolds numbers corresponds to a range of propeller Reynolds numbers, N_v of from $1{\cdot}7 \times 10^6$ to $8{\cdot}5 \times 10^6$, where N_v is based on propeller dimensions.

Thus the maximum N_v value practically covers the 10×10^6 value recommended in Ref. 1, page 307, as being adequate to ensure that model scale effect has been reduced to a negligible amount. The average N_v value for the tests at constant forward Reynolds number of 1×10^6 is about $2{\cdot}5 \times 10^6$.

The deviation of the results for the forward Reynolds number of 3×10^6 from the others in Fig. 7 is a little disturbing as no satisfactory explanation has been found, but it does not invalidate the conclusion which the rest of the evidence provides, *i.e.* that no correction for scale effect need be applied to the results, at low forward Mach numbers at least.

It is not possible to cover a wide range of forward Reynolds numbers at a high forward Mach number in this wind tunnel, so no direct experiment can show whether scale effect is present or not at high Mach numbers. However, a recent report on German high-speed tunnel work does indicate that on aerofoil tests the Reynolds number of the test does influence the behaviour at high Mach number even when the Reynolds number is around 3 or 4×10^6([10]). Thus the possibility of some scale effect at high forward Mach numbers cannot be ruled out entirely from the present series of tests.

Using the method of assessing the scale effect given in R. & M. 1673[2] the maximum deviation of thrust coefficient from the mean value is less than 2 per cent., whilst the average deviation is about 1 per cent.

5.3. *Tests at* $\theta = 50$ *deg. and* 60 *deg.* (*Figs.* 8*a to h*, 9*a to h*).—These tests, which were quite fully done demonstrate the type of result to be expected from propeller tests made using this technique. The magnitude of the random experimental errors is shown by the scatter of the points about the smoothed curves and, except possibly at high M and J values, this is fairly small. The exceptional conditions correspond to the propeller operating near zero thrust and torque at very high forward Mach number thus necessitating the application of relatively very large corrections for tare drag and motor losses to the observed readings, to the detriment of the general accuracy.

Thrust readings were obtained at windmilling conditions with the motor acting as a generator but owing to the absence of reliable information on the electrical losses under such conditions no torque or efficiency values are available. Most of the negative thrust results have been omitted as a consequence.

A point worth noting from the curves under discussion and best exemplified by those of $\theta = 60$ deg. is how the range of J values at which the propulsive efficiency at a given blade angle is at or near its maximum value varies from a wide range at low Mach numbers to a narrow range at high Mach numbers.

6. *Discussion.*—6.1.—The chief interest in the results from tests at $\theta = 50$ deg. and 60 deg. centres round the derived curves given in Figs. 10 to 19 where thrust and torque coefficients are plotted against forward Mach number and tip Mach number at various values of J. Such curves are analogous to the C_L, C_D curves for an aerofoil plotted against M at constant values of incidence and show certain features in common. The plots on a base of tip Mach number are generally more informative than those against forward Mach number and consequently most of the discussion is based upon the former.

6.2. *Tests at* $\theta = 50$ *deg.*—6.21.—In Fig. 10 the most noticeable feature is the rise in both K_T and K_Q values at constant J up to a critical Mach number followed by a steady fall. Both the rise and the fall fit in with the results to be expected from the application of propeller strip theory to the known behaviour of thin aerofoils in compressible flow, in which an increase in lift

coefficient and no appreciable increase in drag coefficient takes place with increase in M at constant incidence. (This applies particularly at low values of incidence; at higher incidences the drag coefficient tends to rise slightly with increase in Mach number.) On approaching the critical Mach number for the section the drag coefficient starts to rise, and at the critical Mach number the lift coefficient falls, accompanied by a much steeper rise in drag coefficient.

It will be noticed in Fig. 10 that very close agreement exists between the observed rise in K_T and the rise predicted by the Glauert theory, when the latter is based on the local Mach number at $0{\cdot}7$ radius. Thus for analysis purposes it seems more satisfactory to base the effective Mach number for the whole blade on the local Mach number at $0{\cdot}7R$ rather than on the tip Mach number.

6.22.—The critical tip Mach numbers at which the peak thrust and torque coefficients occur are more or less constant at the various values of J; in the case of the thrust coefficient this is about $0{\cdot}95$ to $1{\cdot}0$ whilst in the case of the torque coefficient the peak is reached about $0{\cdot}05M$ later. Also, the rate of fall in thrust coefficient once the critical condition has been passed is much faster than the corresponding fall in torque coefficient.

These two effects can be accounted for by consideration of the usual expressions for the thrust and torque of an elementary section of a propeller blade (*see* Ref. 1, page 231).

$$\textit{i.e.}\ \text{Thrust}\ \frac{dT}{dr} = \tfrac{1}{2}Bc\rho W^2\ (C_L \cos\varphi - C_D \sin\varphi).$$

$$\text{Torque}\ \frac{dQ}{dr} = \tfrac{1}{2}Bcr\rho W^2\ (C_L \sin\varphi + C_D \cos\varphi).$$

where

$$\varphi = \tan^{-1}\frac{V}{\Omega r},\ \text{approx.}$$

$$= f(n)J,\ \text{approx.}$$

(Note that φ is of order of 45 deg. or more in the cases under consideration.)

At a given J value the effects of decreasing C_L and increasing C_D as the critical Mach number for the aerofoil is passed are additive in reducing the thrust coefficient, but subtractive in reducing the torque coefficient, thus accounting for the different rates of decrease of the two coefficients. The fact that, at constant incidence, the aerofoil-section drag coefficient usually starts to rise before the lift coefficient falls can account for the peaks in the thrust coefficient occurring slightly earlier than those of the torque coefficients.

This 'phase difference' in critical Mach numbers is well known and is allowed for in the strip theory calculations of propeller performance[3].

6.23.—In the plot of efficiency versus M_{tip} at constant J (Fig. 11) there is a fairly well defined peak at the higher values of J at tip Mach numbers corresponding to the peaks in the thrust and torque coeficient curves. On the other hand, at lower J values, the efficiency drops steadily with increase in tip Mach number. This difference in behaviour with change in J may be attributed to the facts that the simple Glauert law for the increase in lift coefficient with increase in Mach number at constant incidence applies mainly to low values of incidence, that is at the higher J values, and that the drag coefficient is constant at low incidences. At greater incidences (lower J) the relationship between C_L and M tends to become less valid and the drag coefficient does not remain constant but tends to rise with increase in Mach number. Thus one would expect the rise in efficiency with M, if present at all, to be most marked at the higher J values; at lower J values the rise in C_L might be masked by the rise in C_D thus causing a fall in efficiency with increase in Mach number.

6.24.—It will be observed that there is a fair scatter in the cross-plot points on a base of forward Mach number at high values of M (Figs. 12, 13) which could be interpreted to show a

systematic ' waviness ' of the thrust curves at tip Mach numbers beyond the critical. However, no attempt has been made to follow this waviness, and a mean line only has been drawn through the points, as the evidence is felt to be insufficient to justify following the points so closely.

6.3. *Tests at* $\theta = 60$ *deg.*—In the case of the results shown in Figs. 14 to 19 the general characteristics are broadly similar to those already discussed in the preceding paragraphs, though one or two points are worthy of further comment.

The critical tip Mach numbers for the thrust and torque coefficients appear to be about 0·1 less than those for $\theta = 50$ deg., which can be attributed to the fact that for a given tip Mach number, operation at higher values of J with $\theta = 60$ deg. means that more of the blade is shock stalled.

In the plot of efficiency at constant J (Fig. 16) a puzzling feature at certain of the higher values of J is the fall in efficiency followed by a marked peak. Further experimental evidence is required on this point before it can be accepted as genuine. The scatter of the points suggesting waviness of the thrust curves beyond the critical Mach number is more marked but as before, no attempt has been made to follow this apparent systematic waviness.

It might be noted that the very pronounced peak on the $J = 4{\cdot}0$ curve in Fig. 19 is essentially less accurately defined than the others owing to the difficulty already mentioned of maintaining a high degree of accuracy at low values of propeller thrust and torque.

6.4. The remaining curves, Figs. 20, 21, call for little further comment except to remark that the peak efficiency for this propeller reaches 0·9 at low Mach numbers for blade angles of 40 deg. and 50 deg. At 60 deg. blade angle the peak efficiency has dropped to about 0·88 but on the other hand the range of J over which this lower efficiency is attainable is very much wider.

In Fig. 21a it will be seen that the peak efficiency for all blade angles falls off steadily with increase in tip Mach number, whereas the comparable plot of the American results[4] showed a small rise until the critical condition was reached. Also the rate of fall off in efficiency with tip Mach number is much less than the experimental results quoted in Ref. 4 but more nearly akin to the theoretical fall off given in the same paper.

On the basis of forward Mach number (Fig. 21b) the relative positions of the curves are interchanged at high Mach numbers when compared with the same curves in Fig. 21a. That is, the greater blade angles maintain the higher efficiency at high forward Mach numbers. It will be observed that the maximum efficiency begins to fall off at an appreciable rate at a forward Mach number of about 0·6 and from 0·7 onwards it is very rapid indeed, even at the greatest blade setting tested. This rapid fall in efficiency might be delayed by operating at still greater blade angles though to what extent is as yet unknown. A single curve enveloping the individual curves at fixed blade settings shown in the diagram under discussion, would indicate the probable variation of efficiency with forward Mach number of such a propeller operating under normal ' constant speed ' conditions. Thus to determine maximum efficiences for an actual aircraft propeller at Mach numbers of this order still greater blade settings must be tested.

7. *Conclusions.*—The main conclusions from this series of experiments may be summarised as follows.

7.1. The experimental technique for measurement of overall thrust and torque of model propellers in the High Speed Tunnel is satisfactory and gives fairly consistent results, though a more comprehensive calibration of the motor is desirable.

7.2. No appreciable scale effect on thrust or torque coefficient is present at low Mach number, but no evidence is available as to a possible scale effect at high Mach numbers.

7.3. The thrust and torque coefficients and propulsive efficiency results at constant J show no variation of a serious nature from the characteristics to be expected from such a blade section operating at high Mach numbers.

7.4. A maximum efficiency of 0·9 is obtained from this propeller at low forward speeds and tip Mach numbers. With increase in either or both of these parameters the efficiency falls, gradually at first but reaching serious rates of decrease at forward Mach numbers of about 0·7 and upwards. The actual maximum propulsive efficiency at a forward Mach number of 0·7 is about 0·76 which is still quite reasonable and might be capable of still further improvement at greater blade angles.

LIST OF SYMBOLS

D	diameter of propeller (4 ft 6 in).
R	tip radius of propeller.
V	forward speed (corrected).
n	rotational speed, revs/sec.
Ω	rotational speed, radians/sec.
J	rate of advance $= V/nD$.
ρ	density of fluid.
T	thrust.
Q	torque.
K_T	thrust coefficient $= T/\rho n^2 D^4$
K_Q	torque coefficient $= Q/\rho n^2 D^5$
η	propulsive efficiency $= \frac{J}{2\pi} \cdot \frac{K_T}{K_Q}$.
M_u	forward Mach number (uncorrected).
M	forward Mach number (corrected).
M_{tip}	tip Mach number $= M\sqrt{[1 + (\pi/J)^2]}$.
N	tunnel fan rotational speed, revs/min.
RN	forward Reynolds number (based on 1-ft chord).
N_v	propeller Reynolds number (based on propeller dimensions $= \Omega R^2/v$.
γ	kinematic viscosity of fluid.
B	number of blades (2).
W	effective velocity of blade element relative to fluid.
φ	angle of inclination of effective velocity, W, to plane of rotation.
c	chord of blade element.
θ	angle of inclination of blade section datum line to plane of rotation.
r	radius of blade element.

REFERENCES

No.	Author	Title, etc.
1	Durand (Ed.)	Aerodynamic Theory, Vol. IV, J. Springer, Berlin. 1935.
2	Lock and Bateman	Wind-Tunnel Tests of High Pitch Airscrews. Part I. R. & M. 1673 (1934).
3	Conn, Lock, and Pankhurst	Revised Method of Strip Theory Calculations. R. & M. 2035, October, 1945.
4	Stack, Draley, Dclano, and Feldman ..	Investigation of Two-blade Propellers at High Forward Speeds in the N.A.C.A. 8-ft. High Speed Tunnel. Part I. A.R.C. 8051. 1944. NACA. ACR. No. 4A10.
5	Glauert	Wind-Tunnel Interference on Wings, Bodies, and Airscrews. R. & M. 1566 (1933).
6	Young	Note on the Application of the Linear—Perturbation Theory to Determine the Effect of Compressibility on the Wind-Tunnel Constraint on a Propeller. R.A.E. Tech. R. & M. 2113 (1944).
7	Thom	Blockage Corrections and Choking in the R.A.E. High Speed Tunnel R. & M. 2033 (1943).
8	Thom and Jones	Notes on Tunnel Blockage at High Speeds. R. & M. 2385 (1946).
9	Caldwell	Review of the Position of the 200 h.p. Electric Motor for Driving Propellers in the High Speed Tunnel. R.A.E. Tech. Note No. Aero. 1621. 1945.
10	—	Notes on Interrogations of Dr. B. Göthert (D.V.L., Germany). A.R.C. 8880. 1945.
11	Theodorsen	The Theory of Propellers, Part III—Slipstream Contraction with Numerical Values for Two-blade and Four-blade Propellers. N.A.C.A. Report 777 (1944).

APPENDIX I

Notes on Blockage Corrections

By

M. Jones, B.Sc.

The blockage factors are found by the method of images given in R. & M. 2033[7]. The effects of the body and of its images are calculated separately and account is also taken of the propeller, the struts and the motor wake and all their images. In forming the corrections, the effect of everything except the body itself and the thrust wake is eliminated, so that the corrected speed corresponds to the flow through a propeller mounted on an ideal symmetrical body, without struts, of the shape of the motor fairing.

All the blockage effects are calculated for low-speed conditions and are scaled up for compressible flow by the methods given in R. & M. 2113[6] and 2033[7].

In actual practice the various corrections are required in the plane of the propeller disc and for simplicity one representative radius has been chosen, viz. $0{\cdot}7R$. The table of values of blockage corrections at this point is given at the end of the appendix.

Body Solid Blockage.—Regarding the motor as a thin body, the source strength I per unit length necessary to give the model outline, is given approximately by

$$I(x) = U\frac{dA}{dx} = U\pi\frac{dR^2}{dx}$$

where U is the stream velocity, A and R are respectively the area and radius of the body cross section, and x is measured along the stream.

At a point P in the vertical plane through the axis of the body (*see* Fig. 22), the axial component of velocity induced by the source element dx is

$$\delta u = \frac{I(x)\,dx}{4\pi r^2}\cdot\frac{(d-x)}{r}$$

and hence the velocity component induced by the body is

$$u_B = \int_0^l \frac{I(x)\,(d-x)\,dx}{4\pi r^3}$$

$$= \frac{U}{4}\int_0^l \frac{(d-x)\frac{dR^2}{dx}}{[\zeta^2+(d-x)^2]^{3/2}}\,dx$$

where d, ζ, r are as shown in Fig. 22. The integration can be done graphically.

The velocity components induced by the first set of images were calculated in the same way, but in the case of the remaining images, it was found to be sufficiently accurate to replace the body by a source and equal sink on the axis, such that the moment of this system about any line perpendicular to the axis is equal to the moment of the actual distribution.

Thus if q is the strength of the source and sink and $2g$ is the distance between them, then

$$2qg = \pi U\int_0^l x\frac{d}{dx}R^2\,dx = 11\cdot 4U, \text{ numerically.}$$

Taking $g = 45$ in., with the source and sink distant 10 and 100 in. respectively from the nose of the body, gives $q = 1\cdot 52U$ cu ft/sec.

Fig. 24 shows one such image. The axial component of velocity induced at P by the source q is

$$\frac{q\,(d-b)}{4\pi\,[m^2B^2+(nH-\zeta)^2+(d-b)^2]^{3/2}},$$

and by the sink $-q$ is

$$\frac{q\,(b+2g-d)}{4\pi\,[m^2B^2+(nH-\zeta)^2+(b+2g-d)^2]^{3/2}},$$

where the dimensions b, d, ζ are as shown in Fig. 24. B, H are the breadth and height of tunnel and m, n are integers.

Hence the axial velocity induced at P by all such images is

$$u_1 = \frac{4\pi}{q}\,\Sigma\Sigma\left\{\frac{d-b}{[m^2B^2+(nH-\zeta)^2+(d-b)^2]} + \frac{b+2g-d}{[m^2B^2+(nH-\zeta)^2+(b+2g-d)^2]^{3/2}}\right\},$$

where the summation is taken over all pairs of integral values of m and n except $(m=0=n)$ $(m=0,\ n=\pm 1)$ $(m=1,\ n=0)$ and $(m=\pm 1,\ n=\pm 1)$. The series can be summed by the method given in R. & M. 2385.

u_1, together with the components due to the first set of images, gives the total axial velocity u_1 at P due to the images, and the blockage factor then is

$$\varepsilon_B = \frac{u_I}{U}.$$

In order to modify the above calculations for compressible flow, the lengths B, H, ζ should be decreased in the ratio $\beta = \sqrt{(1 - M^2)}$, where M is the Mach number, and the resulting expression for the induced velocity should be multiplied further by the factor $1/\beta$. Thus it would seem a reasonably good approximation to increase the low speed blockage in the ratio $1/\beta x$ where x lies between 3 and 4.

Preliminary measurements of the tunnel wall pressure indicated that the index was much nearer 3 than 4, and accordingly a value of 3 has been chosen. Thus the high speed blockage factor is

$$\varepsilon_B' = \frac{\varepsilon_B}{\beta^3}$$

Struts Solid Blockage.—The solid blockage of the struts is small compared with that of the body, and hence it is a good enough approximation to find the effect of one strut of mean size (chord = 10 in. thickness = 1·32 in., height = 35 in.) in the mean position shown in Fig. 23, and to treble the result.

The image system is shown in Fig. 25. Representing the strut by line sources, the axial velocity induced at P by one such line source CD, of strength q' per unit length, is

$$\frac{q'(d'-g')}{4\pi}\int_{-h}^{+h}\frac{dz}{\{m^2B^2+[(2n-\frac{1}{2})H-\zeta+z]^2+(d'-g')^2\}^{3/2}}$$

$$=\frac{q'(d'-g')}{4\pi[m^2B^2+(d'-g')^2]}\left[\frac{(2n-\frac{1}{2})H-\zeta+h}{\{m^2B^2+[(2n-\frac{1}{2})H-\zeta+h]^2+(d'-g')^2\}^{1/2}}\right.$$

$$\left.-\frac{(2n-\frac{1}{2})H-\zeta-h}{\{m^2B^2+[(2n-\frac{1}{2})H-\zeta+h]^2+(d'-g')^2]^{1/2}}\right]$$

where the dimensions d', g', ζ, h, are as shown in Fig. 25, and B, H are the breadth and height of the tunnel as before.

Summing for all such line sources, and neglecting g' in comparison with d', we obtain

$$\Delta u = \frac{\Sigma\, q'\, g'}{4\pi\,(m^2B^2+d'^2)}\left[\frac{(2n-\frac{1}{2})H-\zeta+h}{\{m^2B^2+[(2n-\frac{1}{2})H-\zeta+h]^2+d'^2\}^{1/2}}\right.$$

$$\left.-\frac{(2n-\frac{1}{2})H-\zeta-h}{\{m^2B^2+[(2n-\frac{1}{2})H-\zeta-h]^2+d'^2\}^{1/2}}\right].$$

Values of q', g' and $\Sigma\, q'g'$ can be found in R. & M. 2033[7], Fig. 4 and finally the velocity component induced by the three struts is

$$u = 3 \times \Sigma\Sigma\, \Delta\, u,$$

where the summation is taken over all pair of values of m and n, and can be performed by the method given in R. & M. 2385[8].

The struts blockage factor then is $\varepsilon_s = u/U$ and at high speeds, this becomes $\varepsilon_s' = \varepsilon_s/\beta^3$.

Wake Blockage.—The usual representation of the wake by a point source and an equal sink a long way downstream is not justified in the case of the airscrew motor since its length is comparable with the tunnel dimensions.

Instead, a triangular distribution of source strength, of total emission corresponding to the C_D values given in Fig. 5*, was assumed along the rear part of the body axis as shown in Fig. 23.

Take the source strength per unit length as

$$q = N(x - s),$$

so that the total emission is

$$Q = N \int_s^l (x - s)\, dx .$$

$$\text{But } Q = \frac{D}{\rho U} = \tfrac{1}{2} C_D\, SU ,$$

where S is the frontal area of the body.

Hence

$$N = \frac{C_D\, SU}{2 \int_s^l (x - s)\, dx} .$$

The images of the wake sources can be treated in the same way as the images of the solid body.

The axial velocity at P due to one image is

$$\Delta u = \frac{N}{4\pi} \left\{ \frac{l - s}{[m^2B^2 + (nH - \zeta)^2 + (d - l)^2]^{1/2}} + \sin h^{-1} \frac{(d - l)}{\sqrt{m^2B^2 + (nH - \zeta)^2}} - \sin h^{-1} \frac{(d - s)}{\sqrt{m^2B^2 + (nH - \zeta)^2}} \right\},$$

and due to the whole image system is

$$u_2 = \Sigma \Sigma\, \Delta\, u ,$$

where the summation is taken over all pairs of values of m and n except $(m = 0 = n)$.

The sinks at infinity induce an axial velocity

$$u_3 = \frac{C_D S}{4BH} ,$$

so that finally, the total axial velocity induced at P is

$$u = u_2 + u_3 ,$$

and the wake blockage is

$$\varepsilon_w = \frac{u}{U} .$$

At high speeds, $\varepsilon_w' = \dfrac{\varepsilon_w}{\beta^3}$.

Effect of Tunnel Walls on Propeller.—On page 299 of Ref. 1, the interference effect of the tunnel walls on a propeller alone is given for incompressible flow as

$$\text{Blockage} \qquad \varepsilon_p = \frac{U'}{U} - 1 = -\frac{\alpha}{2} \frac{\tau}{\sqrt{(1 + 2\tau)}} \text{ approx.}$$

---

* The C_D values given in Fig. 5 include those for the struts, so that the strut wake is in effect included in the body wake. This ignores the fact that C_DS for the struts is approximately half C_DS for the body, and that the corresponding wake is off the tunnel centre line, but since the wake correction is a small fraction of the total, the small error introduced is not thought to be important.

For compressible flow this is adjusted by the methods of R. & M. 2113[6] by including the Mach number as shown

$$\varepsilon_p' = -\frac{\alpha}{2}\frac{\tau}{\sqrt{\left(1+\frac{2\tau}{\beta^2}\right)}}\times\frac{1}{\beta^2}.$$

In the case of this propeller in the H.S.T., $S_A = 15{\cdot}9$ sq ft, tunnel area $= 65$ sq ft and expressing the thrust coefficient as C_T $(= 2\tau)$ for convenience

$$\varepsilon_p' = -\frac{15{\cdot}9}{2\times 65\times 2}\times\frac{C_T}{\sqrt{\left(1+\frac{C_T}{\beta^2}\right)}}\times\frac{1}{\beta^2}$$

$$= -\tfrac{1}{16}\frac{C_T}{\sqrt{\left(1+\frac{C_T}{\beta^2}\right)}}\times\frac{1}{\beta^2}.$$

The value of thrust to be taken in calculating C_T is T_2, the final thrust (*see* Appendix II).

Table 2 below gives values of $(UB/U)\times(1/\beta^3)$, ε_B', ε_s', ε_w' and ε_p' at the point A on the propeller disc at $0{\cdot}7$ radius.

TABLE 2

Individual and total blockage effects at $0{\cdot}7R$ *in the plane of the propeller disc*

M_u	(1) Body	(2) Images of Body $\varepsilon_B' = \varepsilon_B/\beta^3$	(3) Struts and Images $\varepsilon_s' = \varepsilon_s/\beta^3$	(4) Images of Wake $\varepsilon_w' = \varepsilon_w/\beta^3$	(5) Propeller (max. thrust $C_T = 0{\cdot}08$) ε_p'	Effective total (2) + (3) + (4) + (5)	Effective total with zero thrust (2)+(3)+(4)
0·2	−0·0023	0·0098	0·0011	0·0006	−0·0050	0·0065	0·0115
0·3	−0·0025	0·0110	0·0013	0·0007	−0·0052	0·0078	0·0130
0·4	−0·0029	0·0125	0·0014	0·0008	−0·0057	0·0090	0·0147
0·5	−0·0034	0·0148	0·0017	0·0010	−0·0064	0·0111	0·0175
0·6	−0·0043	0·0188	0·0021	0·0011	−0·0075	0·0145	0·0220
0·65	−0·0050	0·0219	0·0025	0·0017	−0·0084	0·0177	0·0261
0·70	−0·0060	0·0264	0·0030	0·0025	−0·0094	0·0225	0·0319
0·72	−0·0066	0·0288	0·0032	0·0036	−0·0100	0·0256	0·0356
0·73	−0·0069	0·0301	0·0034	0·0044	−0·0104	0·0275	0·0379
0·74	−0·0072	0·0315	0·0036	0·0054	−0·0107	0·0298	0·0405
0·75	−0·0076	0·0332	0·0037	0·0068	−0·0110	0·0327	0·0437
0·76	−0·0080	0·0349	0·0040	0·0089	−0·0112	0·0366	0·0478
0·77	−0·0085	0·0370	0·0042	0·0123	−0·0113	0·0422	0·0535
0·78	−0·0090	0·0392	0·0044	0·0172	−0·0116	0·0492	0·0608

The columns of effective total give the fractional amount to be added to the tunnel velocity to give the equivalent free-stream velocity. In the tests carried out it was found that the greatest correction which was applied was 4·7 per cent.

In order to provide experimental checks on the accuracy of the blockage calculations pressure measurements were taken along the tunnel walls and roof and the motor fairing during certain of the experiments (*see* Table 1, section 3 of main report). Prior to these measurements a survey had been made of the wall and roof pressure with the tunnel empty. Analysis of the results has so far proved inconclusive in certain respects and further experiments are required before the results can be published.

LIST OF SYMBOLS FOR APPENDIX I

R radius of cross section of motor.

A area of cross section of motor.

S frontal area of motor

l length of motor.

x distance along axis of motor.

B breadth of tunnel.

H height of tunnel.

S_A area of propeller disc.

α $\dfrac{\text{area of propeller disc}}{\text{cross-sectional area of tunnel.}}$

d, ζ, r *see* Fig. 22.

d' *see* Fig. 25.

U main-stream velocity.

U' equivalent free-stream velocity.

u_B velocity induced by body.

u_I velocity induced by images of body.

ε_B low-speed blockage factor due to the body.

ε'_B high-speed blockage factor due to the body.

ε_s low-speed blockage factor due to the struts.

ε'_s high-speed blockage factor due to the struts.

ε_w low-speed wake blockage.

ε'_w high-speed wake blockage.

ε_p high-speed blockage factor due to the propeller.

M Mach number.

β $= \sqrt{(1 - M^2)}$.

I source strength per unit length along motor axis.

q strength of source and sink representing body.

q' strength per unit length of line sources and sinks representing the struts.

$2g$ distance between source and sink representing the body.

b distance of the source from the nose of the body.

$2g'$ distance between line source and line sink representing strut.

s distance from the nose of the source distribution representing the wake.

C_D drag coefficient.

τ thrust coefficient

$$= \frac{T}{\rho V^2 S_A}$$

C_T thrust coefficient

$$= T/\tfrac{1}{2}\rho V^2 S_A$$

APPENDIX II

Corrections to Thrust Observations

1.1. As explained in section 4.3, the propulsive thrust of the propeller is derived from :—

$$\text{Thrust} = -\text{Observed drag balance reading} + \begin{cases} \text{(i) Tare drag of motor and struts.} \\ \text{(ii) Buoyancy correction due to pressure gradient.} \\ \text{(iii) Correction to (i) for decrease in general field speed caused by propeller blockage.} \\ \text{(iv) Increase in drag of struts due to increased speed in slipstream.} \end{cases}$$

1.2. The evaluation of the tare drag of the motor and struts, item (i), is straightforward from the tests of those items without the propeller, Fig. 5. From this tare drag is subtracted the observed drag reading with the propeller to give a first approximation to the thrust, which is sufficiently close for use with those corrections involving the thrust itself, viz. (ii), (iii), (iv).

$$i.e.,\ T_1 = -\text{observed drag} + \text{tare drag}.$$

The corrections under headings (ii), (iii), and (iv) will now be considered individually.

1.21. *Buoyancy correction.*—When a propeller is developing thrust the working fluid passing through the propeller disc contracts as it moves downstream. In free air this contraction does not affect the pressure of the field of flow outside the wake which remains constant, but in a wind tunnel the presence of the walls requires that the air between the boundary of the wake and the tunnel walls flows in a passage of increasing area in the downstream direction. Thus in a wind tunnel there is a rising pressure gradient in the downstream direction, an effect which is absent when the propeller is operating in free air. Such a pressure gradient acting on the motor body causes a small thrust which can be described as a buoyancy effect.

The magnitude of the pressure gradient may be measured experimentally or calculated approximately ; owing to the absence of reliable experimental data, the latter course has been adopted. In R. & M. 1566[5], page 62, the following equation is given for the buoyancy correction

$$\Delta D = -(A + A')\, dp/dx$$

$$\text{or} \qquad \Delta T = (A + A')\, dp/dx$$

In the present application the value of A' is likely to be very small and can be neglected as the body is well streamlined and of a high fineness ratio (*see* R. & M. 1566[5], page 64 and Fig. 25). The pressure gradient, however, varies considerably in the vicinity of the propeller disc and the best course appears to be to determine the values of the local pressure gradients and use those to determine the correction. Thus

$$\Delta T_1 = \int_0^l \pi y^2 \frac{dp}{dx} \cdot dx .$$

According to R. & M. 2113[6], the pressure rise through a propeller disc in compressible flow is $1/\beta^2$ times the pressure rise through the same disc in incompressible flow for the same thrust. Hence

$$\Delta T_1' = \frac{\pi}{\beta^2} \int_0^l y^2 \frac{dp}{dx} \cdot dx .$$

The total pressure rise through a propeller actuator disc in incompressible flow is

$$p_2 - p_1 = \frac{T}{S_A} .$$

Also, since the momentum along the tunnel is constant to the first order, the ultimate pressure rise can be derived from the thrust as

$$p^3 - p_0 = \frac{T}{C}.$$

Thus the total rise of pressure from the region outside the wake in the plane of the disc to a point far downstream can be taken as $\frac{1}{2}(p_3 - p_0)$. In Ref. 11, Theodorsen gives the results of theoretical calculation of the slipstream contraction with distance downstream for various values of J, and this can be used as a measure of the rate at which the pressure rise outside the wake takes place, *i.e.* to give dp/dx of the equation for buoyancy drag.

Applying Theodorsen's results to the present case the following values for the buoyancy correction are obtained

$$\Delta T_1' = 0{\cdot}012 \frac{T_1}{\beta^2} \quad , \quad \text{for } J = 0.$$

$$= 0{\cdot}0135 \frac{T_1}{\beta^2} \quad , \quad \text{for } J = 1{\cdot}0.$$

$$= 0{\cdot}014 \frac{T_1}{\beta^2} \quad , \quad \text{for } J = 2{\cdot}0.$$

$$= 0{\cdot}0130 \frac{T_1}{\beta^2} \quad , \quad \text{for } J = 3{\cdot}0.$$

$$= 0{\cdot}009 \frac{T_1}{\beta^2} \quad , \quad \text{for } J = 4{\cdot}0.$$

$$= 0 \quad , \quad \text{for } J = 4{\cdot}9.$$

As the bulk of the tests on this propeller were made at J values between 1 and 4 an average value for ΔT_1 has been taken, *i.e.*

$$\Delta T_1' = 0{\cdot}012 \frac{T_1}{\beta^2}.$$

This correction is *subtracted* from the approximate thrust T_1.

1.2.2. *Propeller Blockage Correction**.—A propeller running in a closed wind tunnel causes a blockage effect such that the general flow in the working section is slowed down. Hence the tare drag, obtained from the calibration curve of Fig. 5 in conjunction with uncorrected values of $\frac{1}{2}\rho V^2$ from the tunnel pressure readings will be overestimated because of this blockage effect. The true thrust of the propeller under these conditions is obtained by comparing the tare drag and the observed drag at the same corrected tunnel speed. In practice it is found to be more convenient to compare them at the same uncorrected speed, than to apply a separate blockage correction to the thrust.

Reverting to the basic expressions for the thrust, section 1.1:—

1st approximation : Thrust $T_1 = -D + D_0$

Sections 1.2.2 and 1.2.3 were revised as R.A.E. Report Aero. 2096a to replace those appearing in the original R.A.E. Report Aero. 2096.

* This now includes the Addendum by Thomson which formed part of the original R.A.E. Report.

If ΔV is that part of the blockage correction produced by the propeller thrust, then this correction to the thrust is

$$\Delta T_2 = \Delta D_0 = \Delta V \cdot \frac{dD_0}{dV}.$$

Writing $D_0 = \frac{1}{2}\rho V^2 C_{D0} S.$

Then $\Delta T_2 = \Delta(\frac{1}{2}\rho V^2 C_{D0} S),$

or
$$\Delta T_2' = D_0 \left\{ \frac{\Delta \frac{1}{2}\rho V^2}{\frac{1}{2}\rho V^2} + \frac{\Delta C_{D0}}{C_{D0}} \right\}$$
$$= D_0 \left\{ \left(\frac{\Delta \frac{1}{2}\rho V^2}{\frac{1}{2}\rho V^2} \right) + \left(\frac{\Delta M_u}{M_u} \times \frac{M_u}{C_{D0}} \times \frac{dC_{D0}}{dM_u} \right) \right\},$$

allowing for the effect of compressibility on both $\frac{1}{2}\rho V^2$ and C_{D0}.

Now, for normal blockage corrections,

$$\frac{\Delta \frac{1}{2}\rho V^2}{\frac{1}{2}\rho V^2} = (2 - M_u^2)\varepsilon$$

and
$$\frac{\Delta M_u}{M_u} = (1 + \tfrac{1}{5}M_u^2)\varepsilon .$$

Hence
$$\Delta T_2' = D_0 \varepsilon \left\{ (2 - M_u^2) + (1 + \tfrac{1}{5}M_u^2) \frac{M_u}{C_{D0}} \cdot \frac{dC_{D0}}{dM_u} \right\}.$$

In Appendix I, the propeller blockage is given as

$$\varepsilon_p' = -\tfrac{1}{16} \times \frac{C_T}{\sqrt{\left(1 + \frac{C_T}{\beta^2}\right)}} \times \frac{1}{\beta^2}.$$

For the present application this expression can be simplified by assuming C_T to be small (it never exceeded 0·03 at high values of M).

Hence
$$\varepsilon_p' = -\tfrac{1}{16} \cdot \frac{C_T}{\beta^2} = -\tfrac{1}{16} \cdot \frac{T_1}{\frac{1}{2}\rho V^2 S_A \beta^2}.$$

Finally :

$$\Delta T_2' = D_0 \times -\tfrac{1}{16} \cdot \frac{T_1}{\frac{1}{2}\rho V^2 S_A \beta^2} \left\{ (2 - M_u^2) + (1 + \tfrac{1}{5}M_u^2) \frac{M_u}{C_{D0}} \cdot \frac{dC_{D0}}{dM_u} \right\}.$$
$$= \frac{C_{D0} T_1}{16 \left(\frac{S_A}{S}\right) \beta^2} \left\{ (2 - M_u^2) + (1 + \tfrac{1}{5}M_u^2) \frac{M_u}{C_{D0}} \cdot \frac{dC_{D0}}{dM_u} \right\}$$
$$= -\frac{C_{D0}}{126} \cdot T_1 \times \frac{1}{1 - M_u^2} \left\{ (2 - M_u^2) + (1 + \tfrac{1}{5}M_u^2) \frac{M_u}{C_{D0}} \cdot \frac{dC_{D0}}{dM_u} \right\}.$$

This correction is *subtracted* from the approximate thrust T_1.

1.2.3. *Change of Drag due to Slipstream.*—This correction takes account of the change in drag of the body and strut assembly due to the increased drag of that part of the assembly exposed to the propeller slipstream.

It has been based on the following assumptions :—

(*a*) That the slipstream diameter is constant and equal to the propeller diameter.

(*b*) That the ratio of the $C_D S$ value for the exposed portion of the struts and the total $C_D S$ for motor and strut assembly can be calculated for low speeds and that this ratio holds at high speeds.

(*Note.*—This assumption disregards possible changes in the relative contribution of the struts, motor body and interference drags between low and high speeds. An examination of this has

been made in some later work[12] and the conclusion reached is that changes within the probable limits do not have any appreciable effect up to the forward Mach numbers now being considered.)

Assuming also that transition occurs on the struts rather earlier than 0·1 chord, then by calculation of the drag of the struts and measurement of the total drag :—

$$\frac{C_D S \text{ (exp.)}}{C_D S \text{ (total)}} = 0{\cdot}2 = K, \text{ say.}$$

And, in free air,

$$\frac{\text{Slipstream speed}}{\text{free stream speed}} \cdot \frac{V_S}{V} = \sqrt{\left\{1 + \frac{T_1}{\frac{1}{2}\rho V^2 S_A}\right\}} = 1 + \varepsilon_S \ldots$$

Therefore $$\varepsilon_S \simeq \frac{T_1}{\rho V^2 S_A} \text{ — assuming the thrust coefficient to be small.}$$

Therefore, following section 1.2.2:—

$$\begin{aligned}\Delta T_3' &= K D_0\, \varepsilon_S \left\{(2 - M_u^2) + (1 + \tfrac{1}{5}M_u^2)\frac{M_u}{C_{D0}} \cdot \frac{dC_{D0}}{dM_u}\right\} \\ &= K \tfrac{1}{2}\rho V^2 C_{D0}\, S \frac{T_1}{\rho V^2 S_A} \cdot \left\{(2 - M_u^2) + (1 + \tfrac{1}{5}M_u^2)\frac{M_u}{C_{D0}} \cdot \frac{dC_{D0}}{dM_u}\right\} \\ &= \frac{C_{D0}\, T_1}{79}\left\{(2 - M_u^2) + (1 + \tfrac{1}{5}M_u^2)\frac{M_u}{C_{D0}} \cdot \frac{dC_{D0}}{dM_u}\right\}.\end{aligned}$$

This correction is *added* to the approximate thrust T_1.

(*Note.*—It does not contain the factor $\{1/(1 - M_u^2)\}$ as the propeller blockage does; this is because the velocity increment in the slipstream for a given propeller thrust coefficient is independent of M (*see* R. & M. 2113[6]).)

1.2.4. Summing up, the corrections under headings (ii), (iii) and (iv) of the thrust equations are:—

$$\begin{aligned}\Delta T_1' + \Delta T_2' + \Delta T_3' = \Delta T' = &- 0{\cdot}012\frac{T_1}{\beta^2} - \frac{C_{D0}}{126}\frac{T_1}{\beta^2}\left\{(2 - M_u^2) + (1 + \tfrac{1}{5}M_u^2)\frac{M_u}{C_{D0}} \cdot \frac{dC_{D0}}{dM_u}\right\} \\ &+ \frac{C_{D0}\, T_1}{79}\left\{(2 - M_u^2) + (1 + \tfrac{1}{5}M_u^2)\frac{M_u}{C_{D0}} \cdot \frac{dC_{D0}}{dM_u}\right\}.\end{aligned}$$

The resultant correction to be *added* to T_1.

The contribution of each of the above items as a fraction of the thrust T_1 at various values of M is given in tabular form below :—

TABLE 3

Corrections to Thrust

M_u	C_{D0}	Buoyancy correction $\Delta T_1'/T_1$	Prop. blockage correction $\Delta T_2'/T_1$	Slipstream correction $\Delta T_3'/T_1$	Net correction $\Delta T'/T_1$
0·2	0·1083	−0·0120	−0·00175	+0·002708	−0·0110
0·3	0·1086	−0·0132	−0·00183	+0·002675	−0·0124
0·4	0·1104	−0·0141	−0·00206	+0·00279	−0·0134
0·5	0·1147	−0·0161	−0·00248	+0·00295	−0·0156
0·6	0·1225	−0·0187	−0·00338	+0·00343	−0·0187
0·65	0·1310	−0·0208	−0·00584	+0·00539	−0·0213
0·70	0·1670	−0·0235	−0·02038	+0·01656	−0·0273
0·72	0·2260	−0·0250	−0·0532	+0·0408	−0·0374
0·73	0·2600	−0·0258	−0·0644	+0·0478	−0·0424
0·74	0·3050	−0·0266	−0·0747	+0·0535	−0·0478
0·75	0·3650	−0·0277	−0·1058	+0·0732	−0·0603

LIST OF SYMBOLS FOR APPENDIX II

A	volume of body.
A'	virtual volume of body in accelerated flow.
$\frac{dp}{dx}$	Longitudinal pressure gradient.
ΔD	buoyancy drag.
D	observed drag.
D_0	tare drag.
C_{D0}	tare-drag thrust coefficient.
ΔT_1	thrust correction for buoyancy effect in incompressible flow.
$\Delta T_1'$	thrust correction for buoyancy effect in compressible flow.
l	length of body.
y	radius of body at distance x from propeller disc.
M_u	uncorrected Mach number.
β	$1 - M_u^2$.
T	thrust.
S_A	propeller-disc area.
C	tunnel cross-sectional area.
p_0	initial pressure far upstream of propeller disc
p_1	pressure immediately before propeller disc.
p_2	pressure immediately after propeller disc.
p_3	final pressure far downstream from propeller disc.
ΔT_2	thrust correction for field speed (incompressible flow).
$\Delta T_2'$	thrust correction for field speed (compressible flow).
ΔV	velocity increment.
ε_p'	blockage factor on general field speed due to propeller (compressible flow).
C_T	propeller-thrust coefficient $= T_1/\frac{1}{2}\rho V^2 S_A$.
V_S	slipstream speed.
ε_S	blockage factor due to slipstream.
$\Delta T_3'$	correction factor due to slipstream effect on struts (compressible flow).

APPENDIX III

Calibration of Motor

1.1. The motor is calibrated on the dynamometer stand by measuring the electrical power input and the mechanical power output. The difference between the two quantities, *i.e.* the motor loss, is separated into its constituent parts by the usual methods employed in electrical engineering. Hence when driving a propeller in the tunnel the motor b.h.p. is obtained by subtraction of the aggregate losses under the observed operating conditions from the electrical input.

1.2. The quantities observed during a calibration run are therefore :—

Electrical power input.
Applied voltage.
Stator current.
Stator winding temperature.
r.p.m.
Slip frequency.
Brake load.

In addition, the brine coolant inlet and outlet and bearing temperatures are noted.

From this data it is possible to separate the losses into :—

(a) those independent of winding temperature for a given input power and frequency (*i.e.* speed). These are the iron friction and windage, and stray losses.

and (b) those dependent upon winding temperature for a given input power and frequency.

These comprise the copper losses which are determined by

(i) Stator copper loss $= I^2 R_0 (1 + \alpha T)$

(ii) Rotor copper loss $=$ Input power $\times$ slip
$= W \times \sigma$

In addition there is an extra loss when the motor is in the wind-tunnel driving a propeller due to the axial load on the bearings. This is termed the thrust loss, but is very small.

1.3. The procedure followed was first to establish the voltage/r.p.m. ratio which gave the minimum losses at constant b.h.p., this value being used throughout all tests. Secondly by running at constant torque and r.p.m. for a protracted period whilst the motor was heating up, to determine whether in fact the losses could be separated into the categories of copper and iron losses, being dependent and independent respectively of the stator winding temperature.

This latter experiment did not give completely satisfactory results as it appeared as though the iron losses too were dependent upon temperature to a slight degree. In view of the rather brief tests which were made in the available time, and as the motor was due to be modified later, the validity of the proposed loss analysis method was accepted. Future calibration will be rather more exhaustive.

A series of runs at constant r.p.m. and varying torque were made to cover the likely operating range of the motor and the various losses calculated. These were analysed and presented in a form suitable for use in subsequent tunnel tests. The method adopted was to plot the total losses (except the thrust loss, see later) at 0 deg. C. stator winding temperature (losses L) for given r.p.m. and input power values and to plot a second series of curves comprising the losses requiring temperature correction (losses l) at 0 deg. C. on the same basis also. These latter were corrected for the difference of the observed stator temperature from 0 deg. C. by multiplying l by the temperature coefficient times temperature difference and then adding to the total losses L.

Hence total losses $= L + (l \times \alpha \times$ temperature difference from 0 deg. C.).

A chart illustrating the method of determining the losses for a given running condition is given in Fig. 26. The thrust loss was determined by the motor manufacturers over the range of thrust values likely to be encountered in practice and can be expressed as

$$\text{Thrust loss in watts per 1,000 r.p.m.} = 0{\cdot}033 \times \text{thrust in lb.}$$

This is negligibly small in practice.

1.4. It should be noted that the present calibration of the motor shows that the iron losses are rather high and that excessive heating of the steel end rings clamping the rotor copper bars occurs[9]. This has had the result that the present calibration is not so consistent as is desirable.

It is hoped that by modifying these end rings, the iron losses and the overheating will be appreciably reduced and thus the overall losses will be reduced with consequent improvement in the reliability of the method.

LIST OF SYBMOLS FOR APPENDIX III

I	motor current.
T	stator-winding temperature.
R_0	stator-winding resistance at 0 deg. C.
α	temperature coefficient of resistance of copper.
σ	fractional slip.
W	input power in watts.
L	total losses (except thrust loss).
l	losses requiring temperature correction.

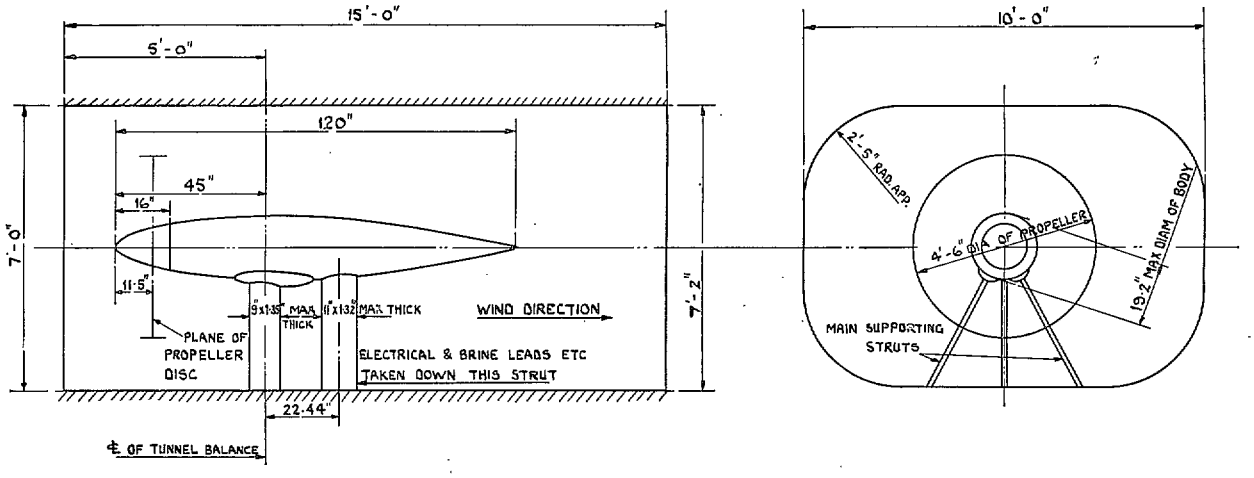

FIG. 1. Outline of 200 h.p. propeller motor in H.S.T. working section.

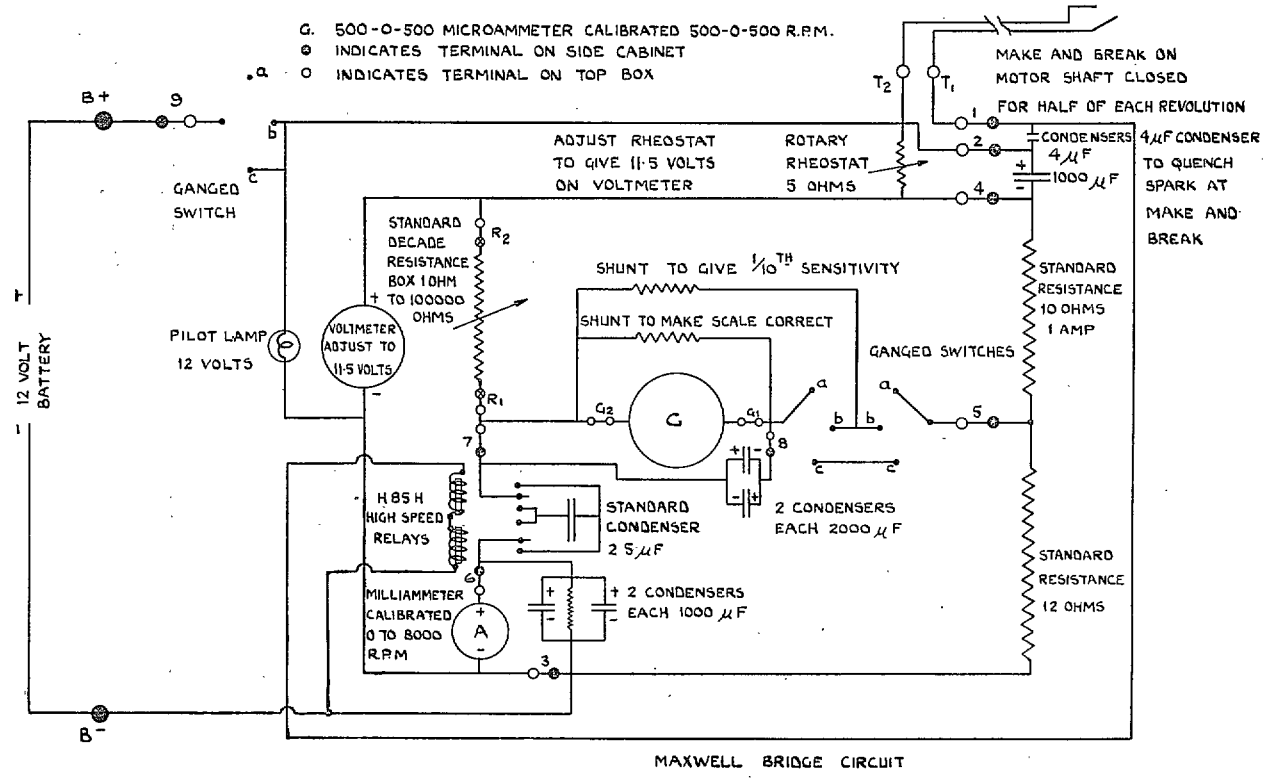

FIG. 2. R.P.M. indicator for propeller motor. Range 500 to 8,000 r.p.m.

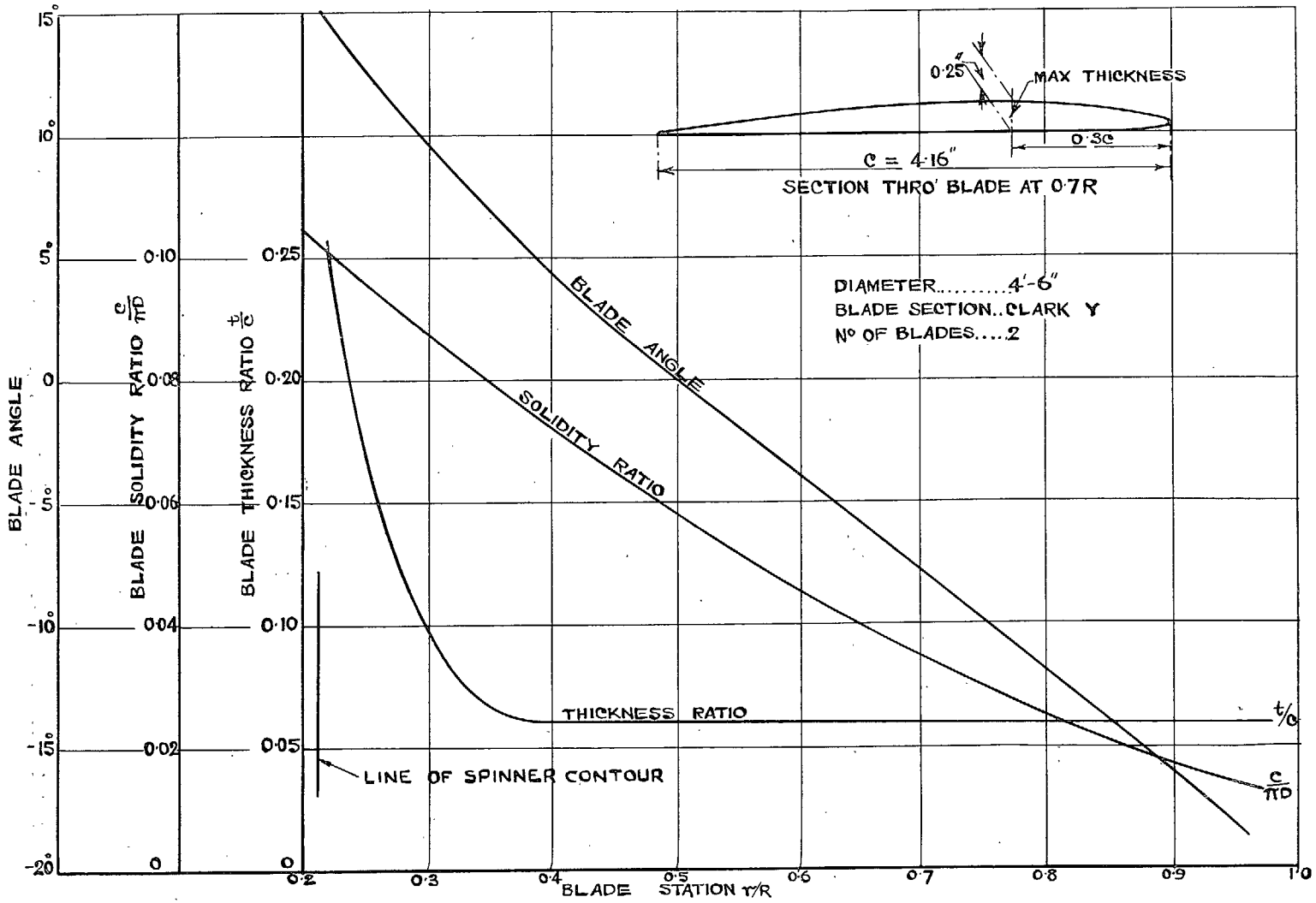

FIG. 3. Basic details of propeller.

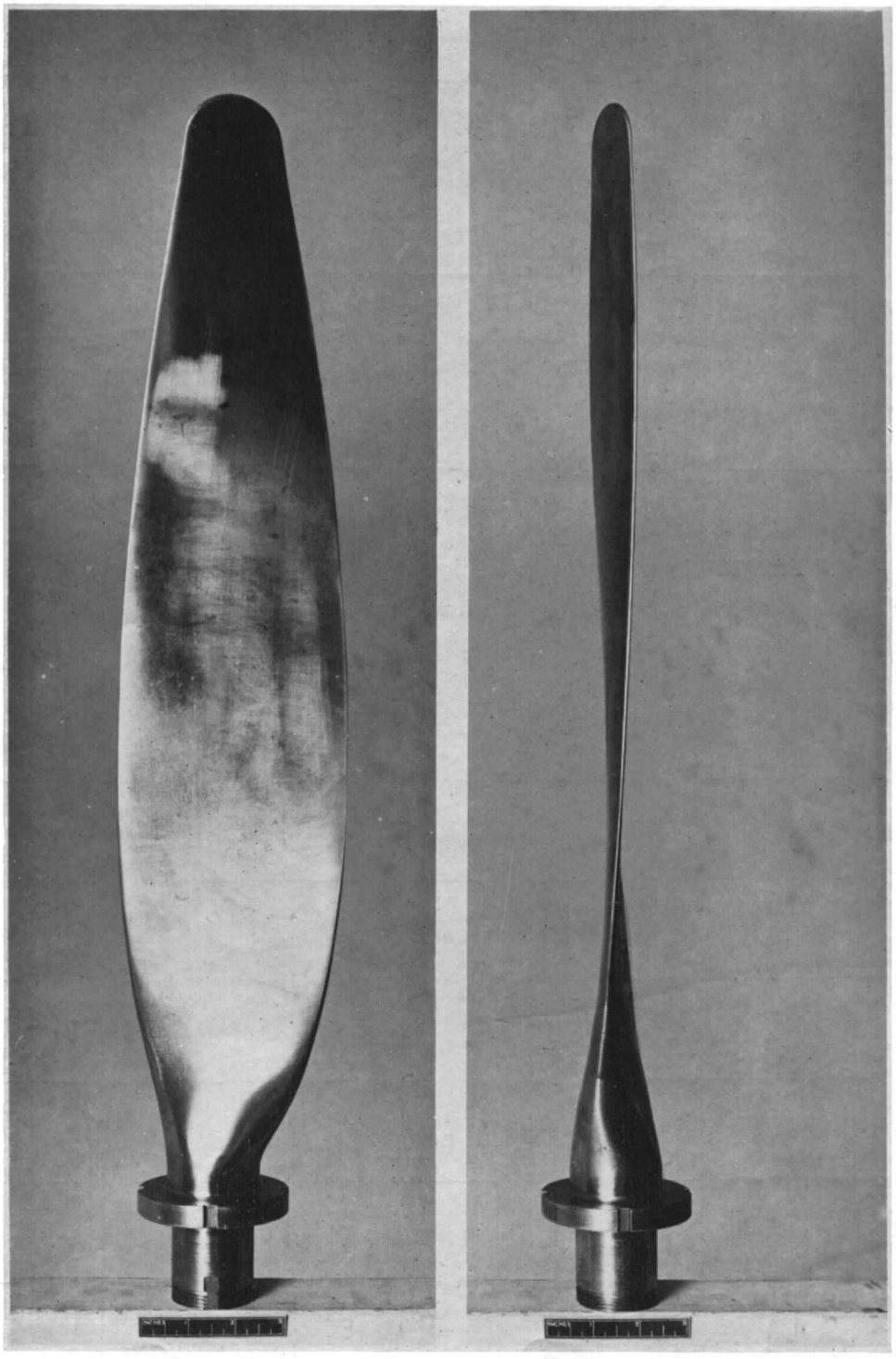

FIG. 4. Number 0 Propeller Blade.

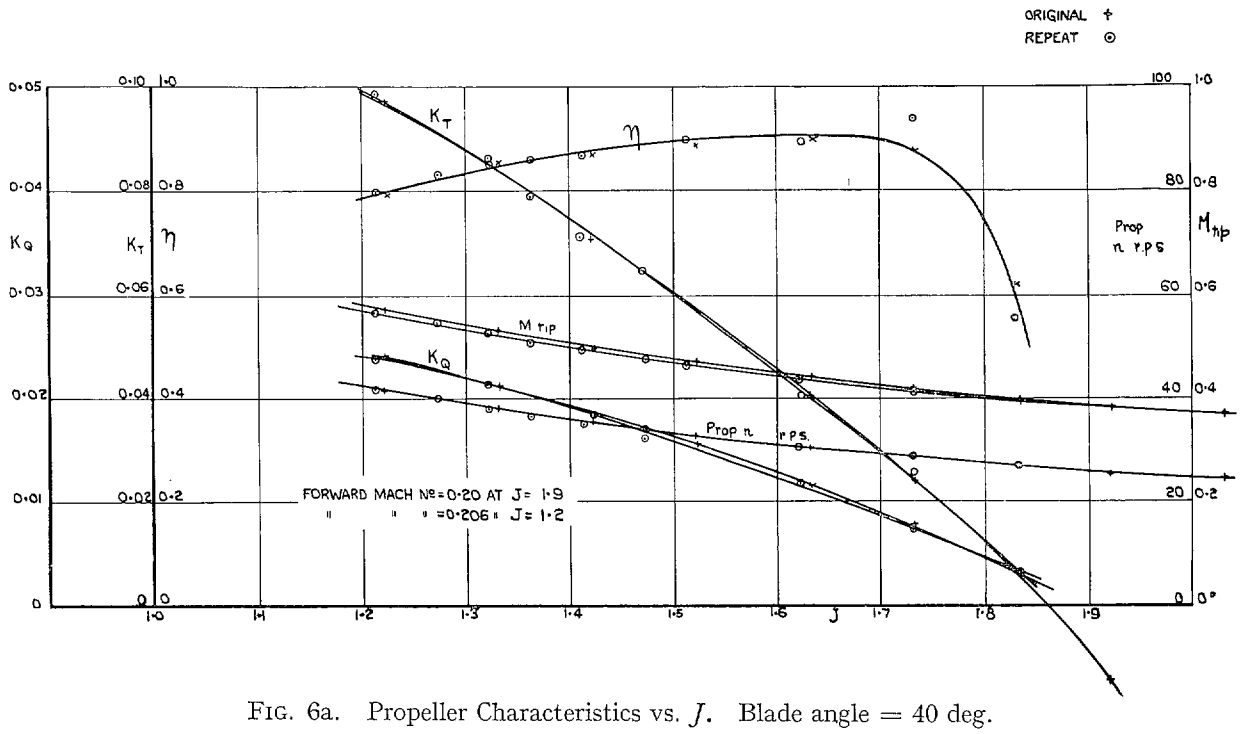

FIG. 6a. Propeller Characteristics vs. J. Blade angle = 40 deg.
Forward Mach number = 0·2.

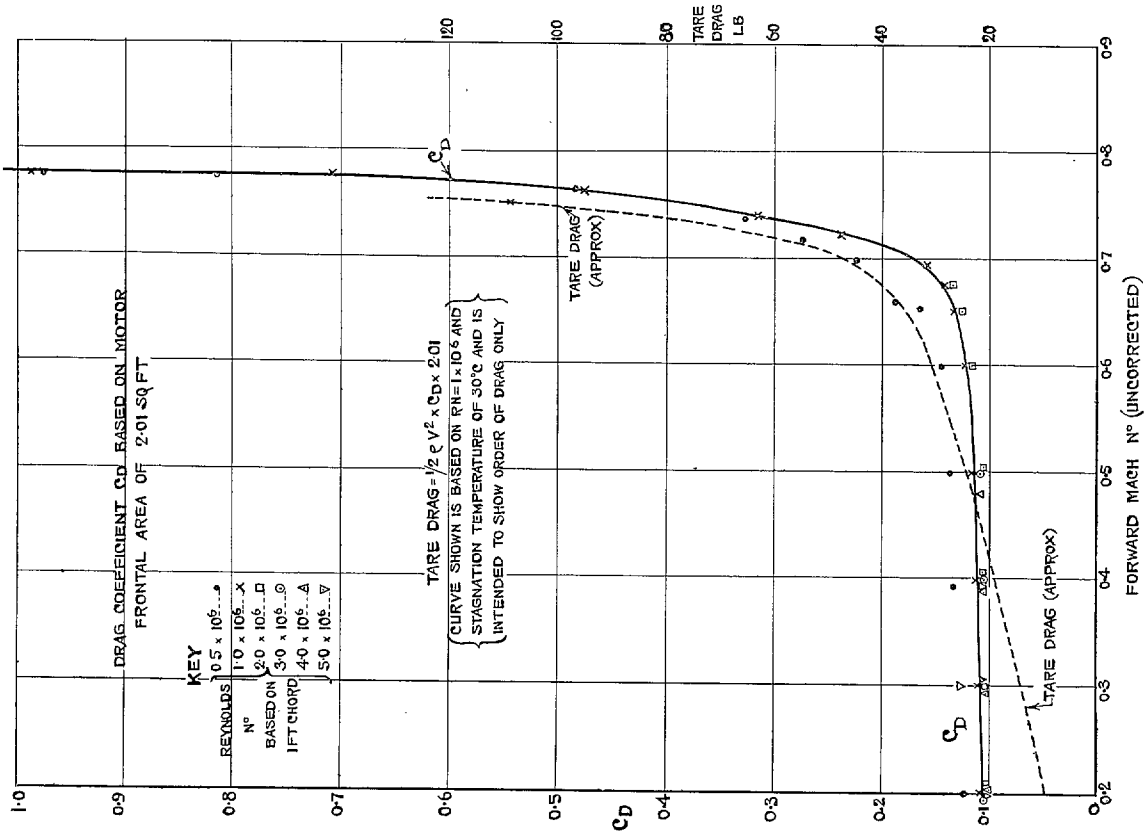

FIG. 5. Tare drag of motor and struts at various Reynolds numbers.

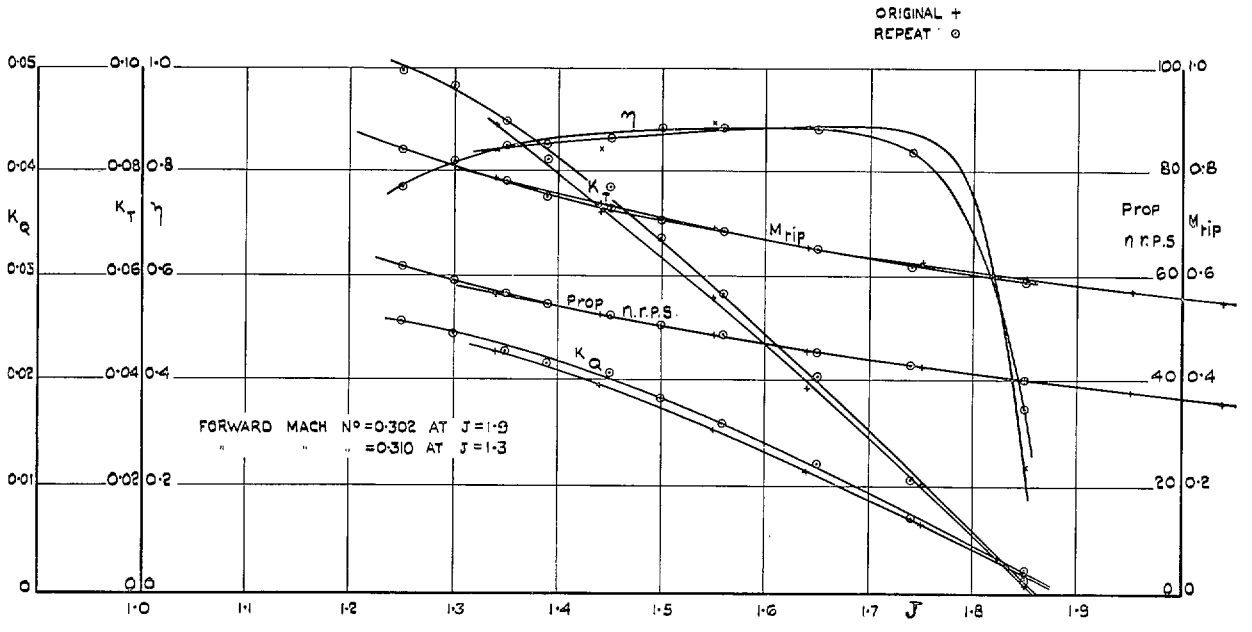

FIG. 6b. Propeller Characteristics vs. J. Blade angle = 40 deg.
Forward Mach number = 0·3.

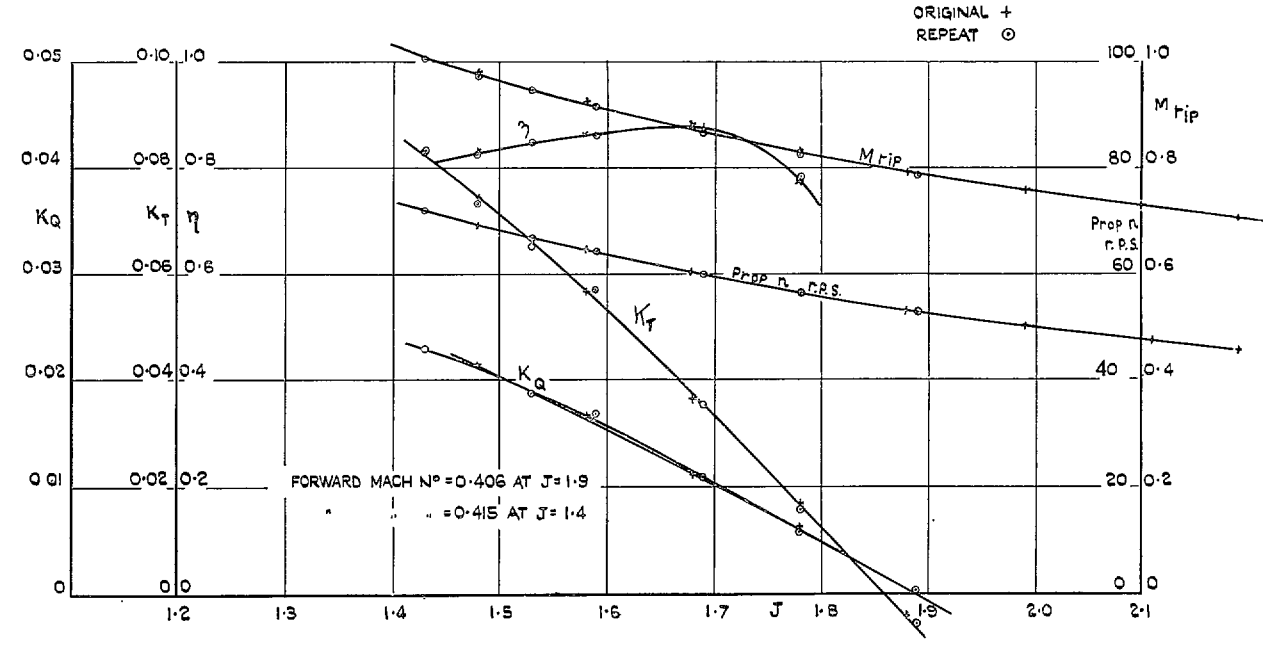

FIG. 6c. Propeller Characteristics vs. J. Blade angle = 40 deg.
Forward Mach number = 0·41.

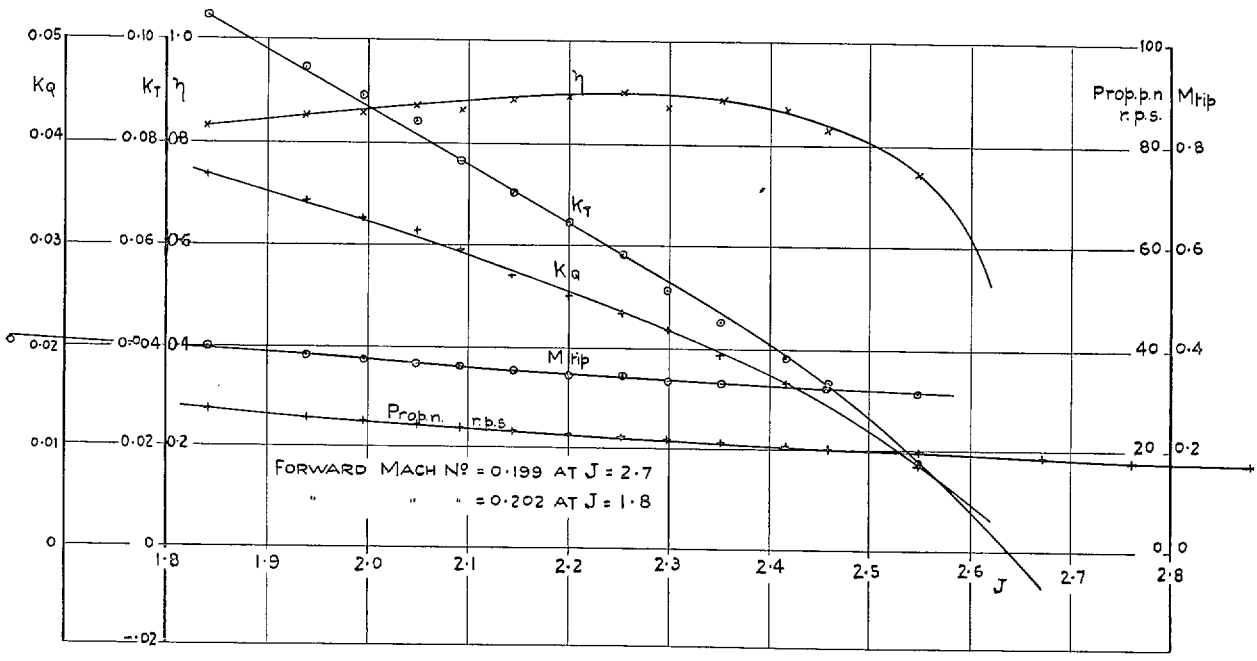

FIG. 8a. Propeller Characteristics vs. J. Blade angle = 50 deg.
Forward Mach number = 0·2.

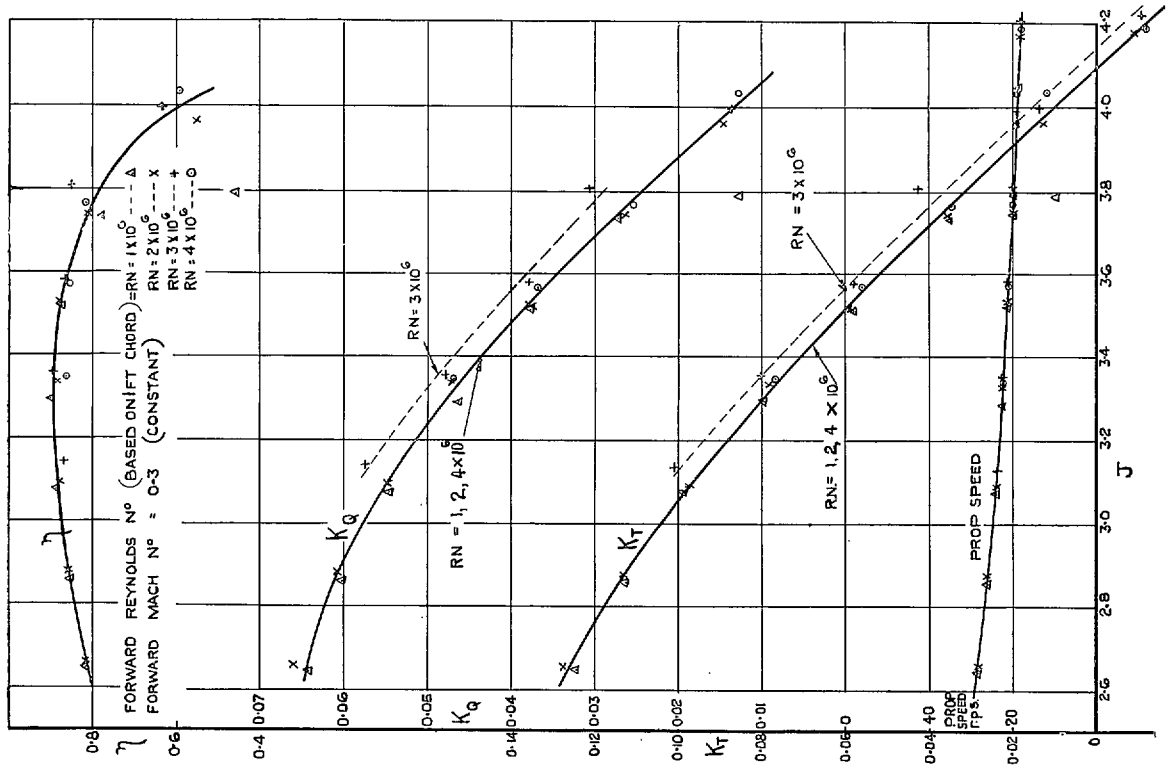

FIG. 7. Propeller Characteristics vs. J at constant Forward Mach number for Various Forward Reynolds numbers.

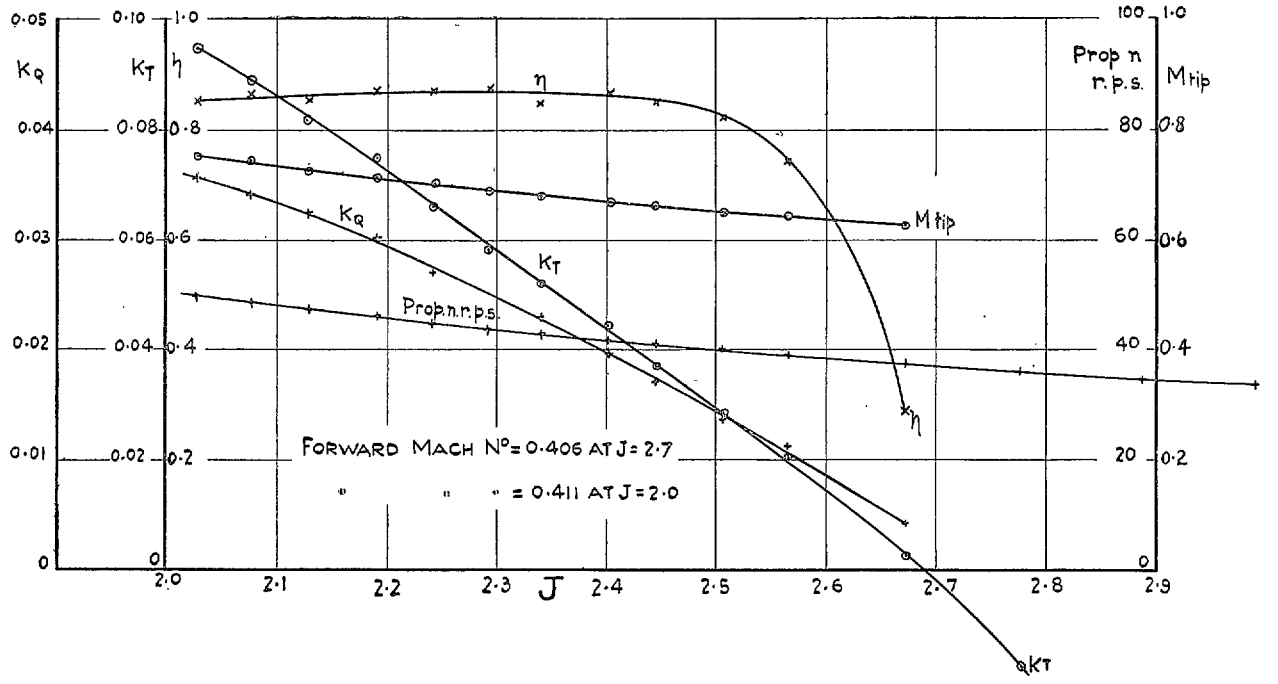

FIG. 8b. Propeller Characteristics vs. J. Blade angle = 50 deg.
Forward Mach number = 0·41.

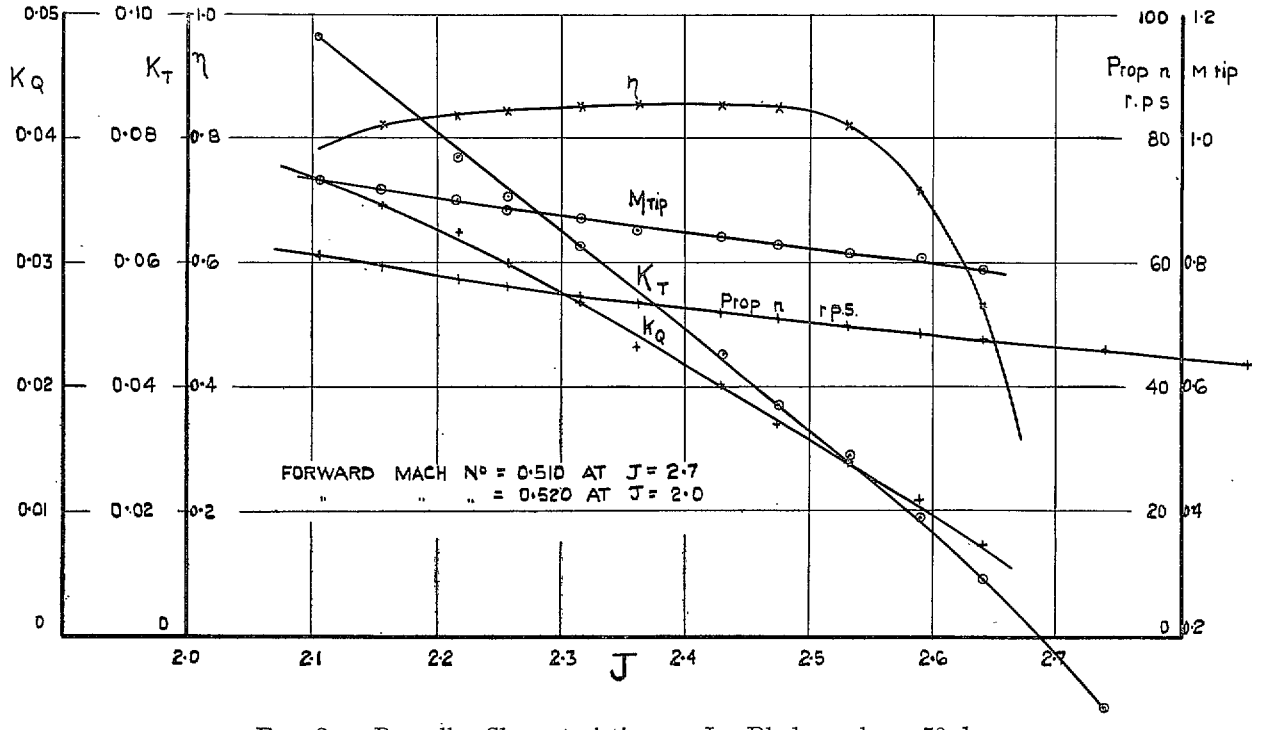

FIG. 8c. Propeller Characteristics vs. J. Blade angle = 50 deg.
Forward Mach number = 0·51.

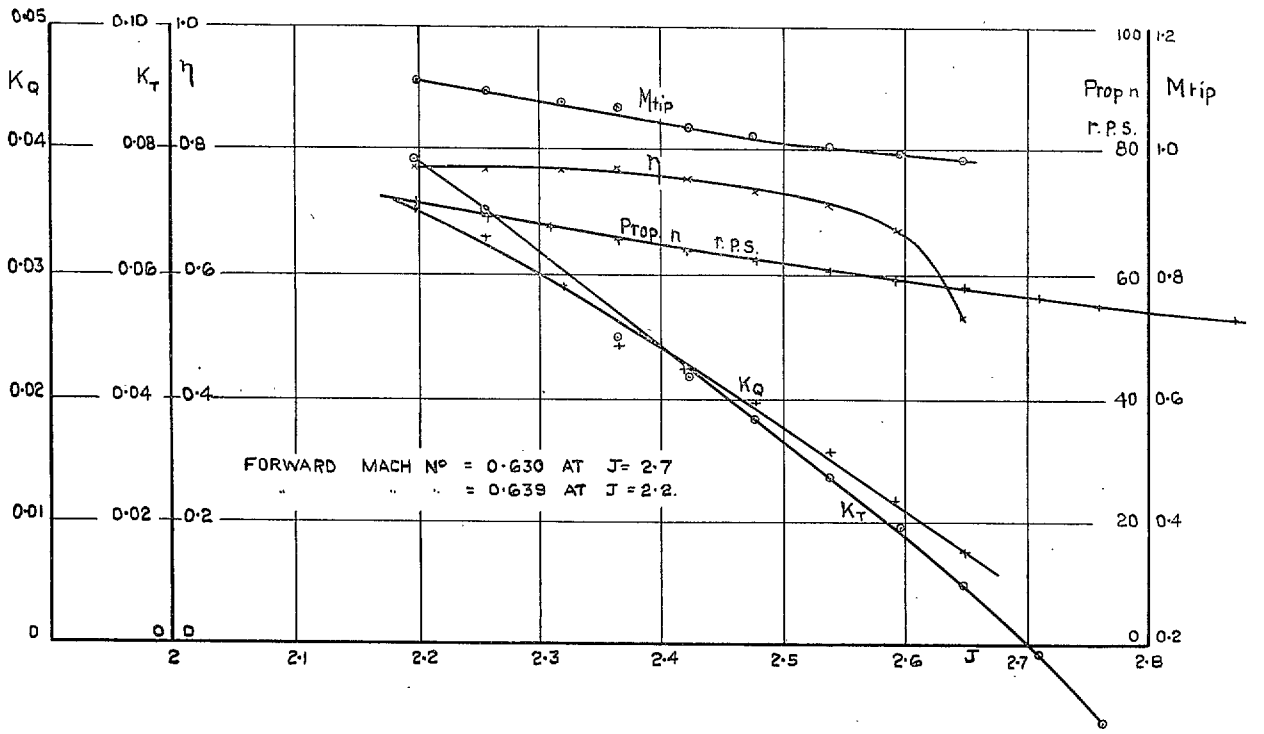

FIG. 8d. Propeller Characteristics vs. J. Blade angle = 50 deg.
Forward Mach number = 0·63.

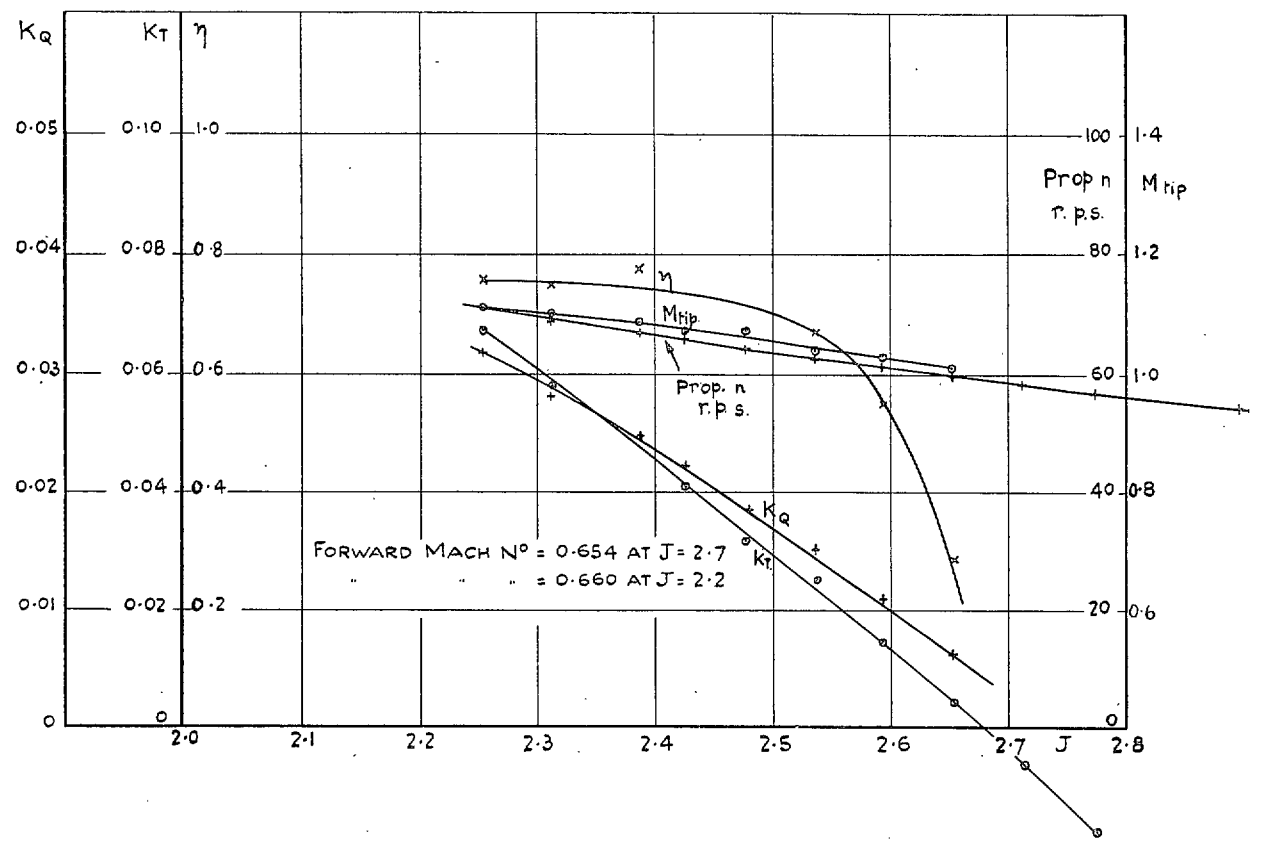

FIG. 8e. Propeller Characteristics vs. J. Blade angle = 50 deg.
Forward Mach number = 0·66.

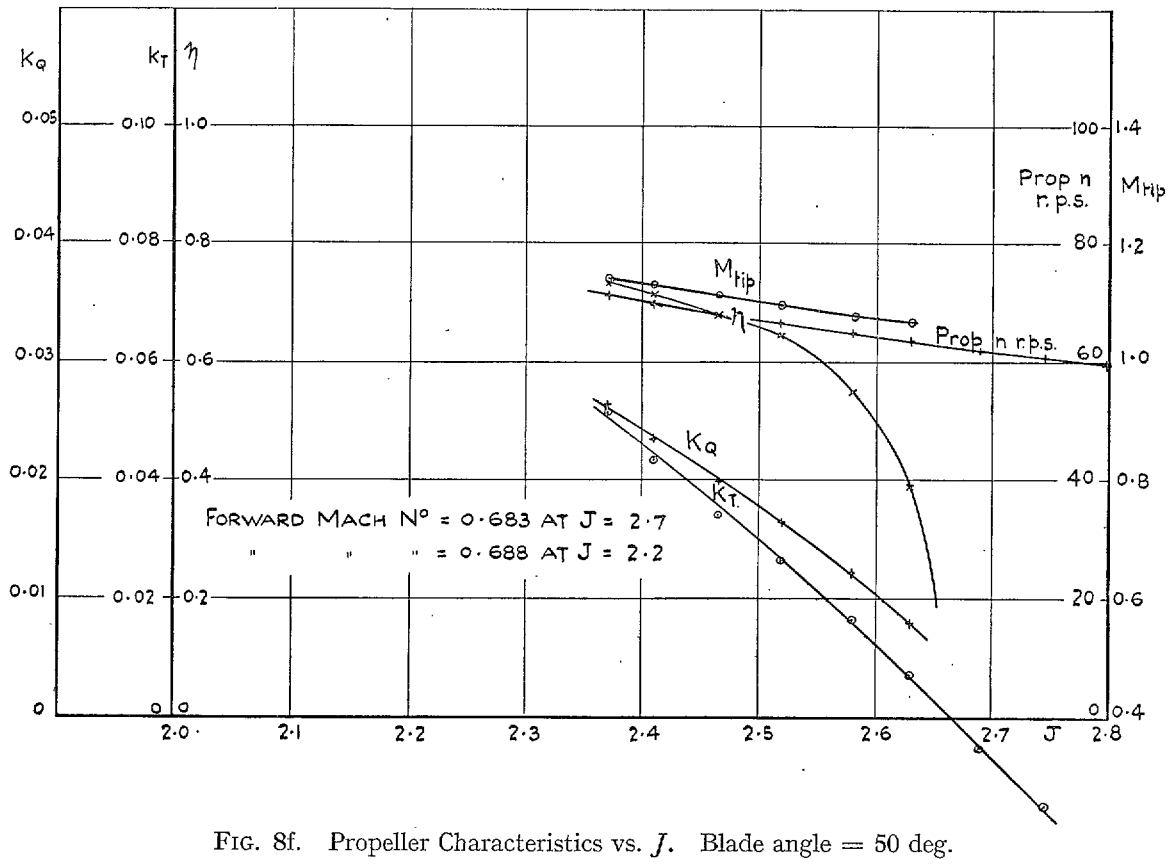

FIG. 8f. Propeller Characteristics vs. J. Blade angle = 50 deg.
Forward Mach number = 0·685.

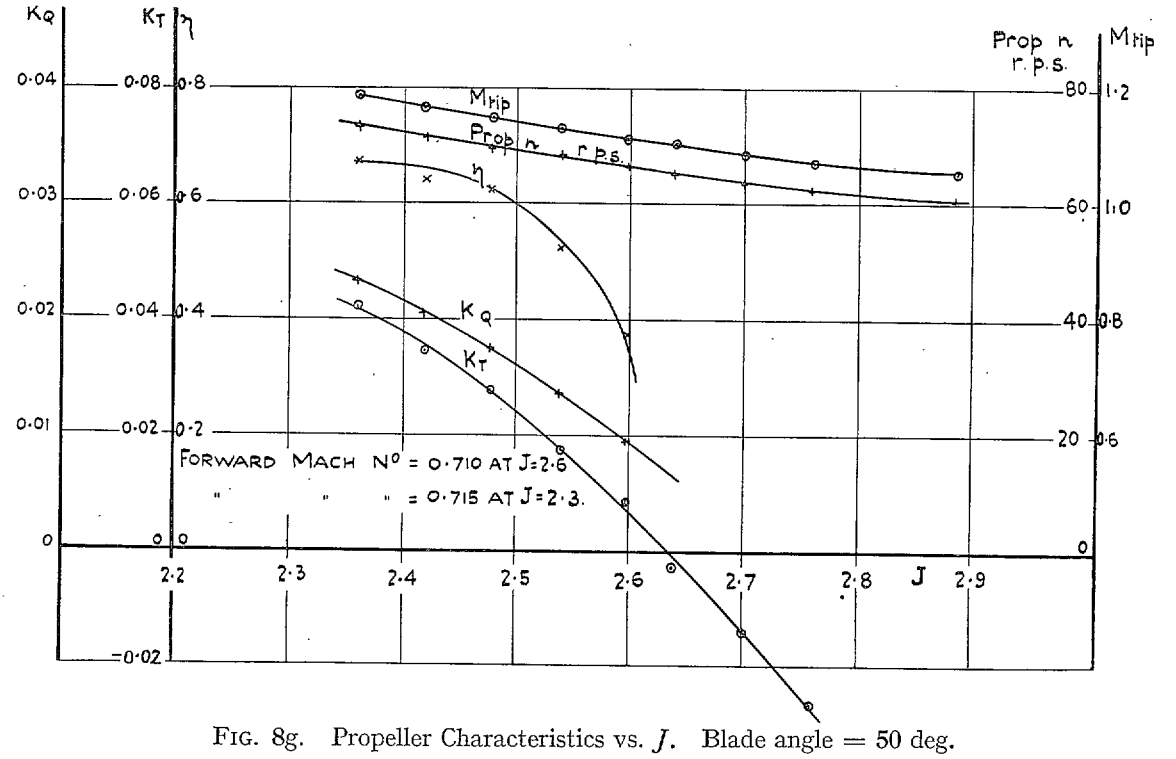

FIG. 8g. Propeller Characteristics vs. J. Blade angle = 50 deg.
Forward Mach number = 0·715.

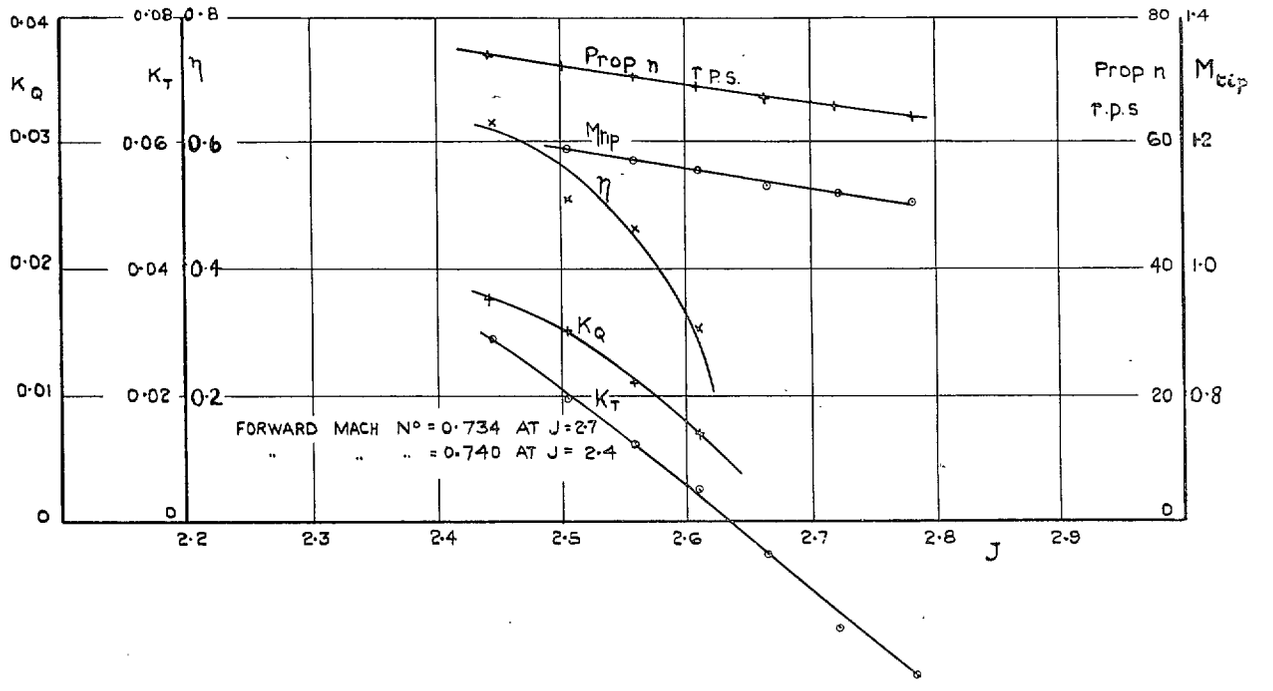

FIG. 8h. Propeller Characteristics vs. J. Blade angle = 50 deg.
Forward Mach number = 0·74.

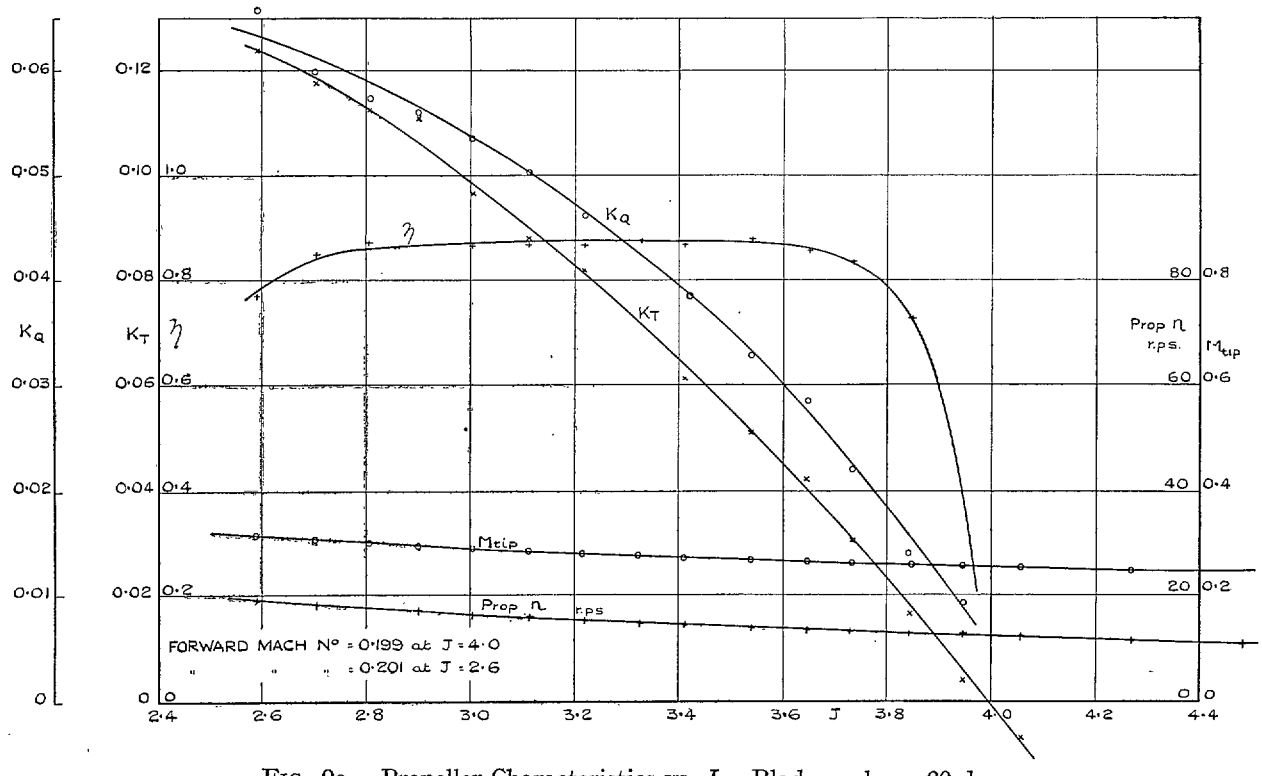

FIG. 9a. Propeller Characteristics vs. J. Blade angle = 60 deg.
Forward Mach number = 0·2.

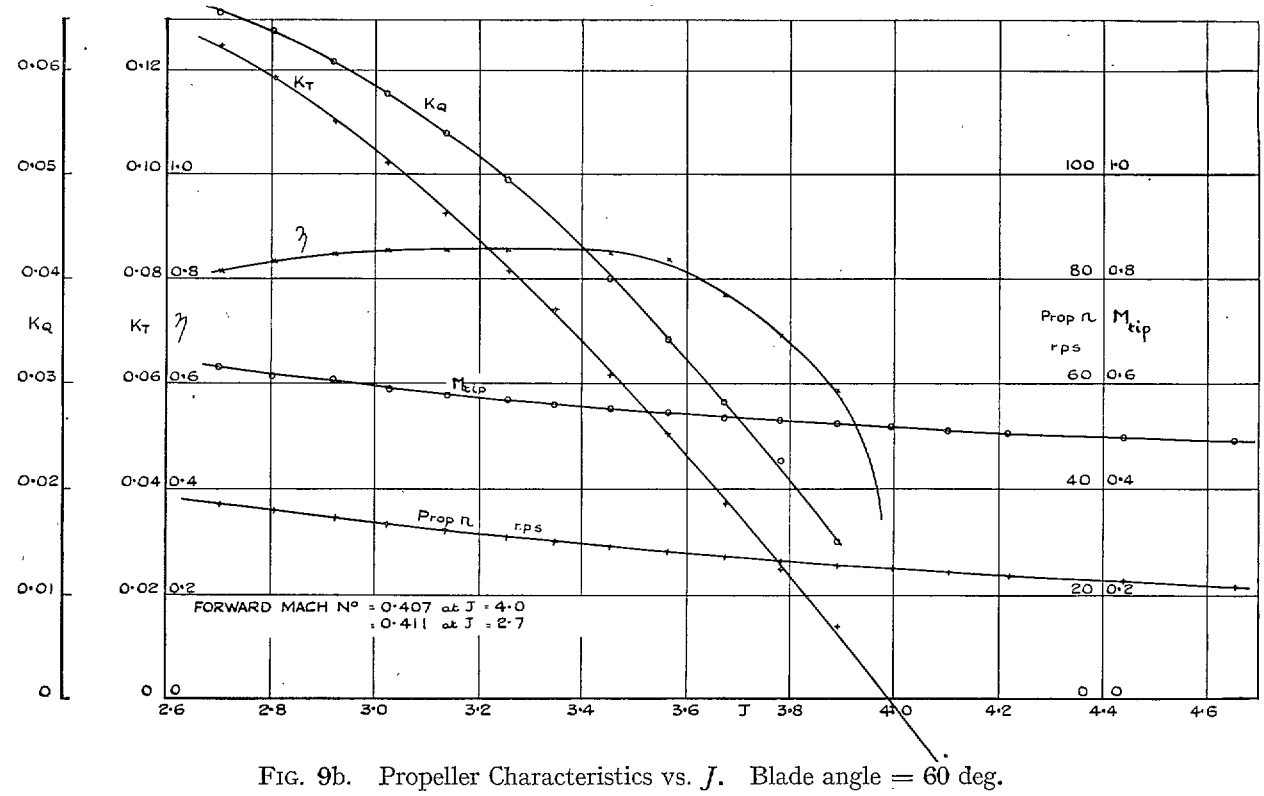

FIG. 9b. Propeller Characteristics vs. J. Blade angle = 60 deg.
Forward Mach number = 0·41.

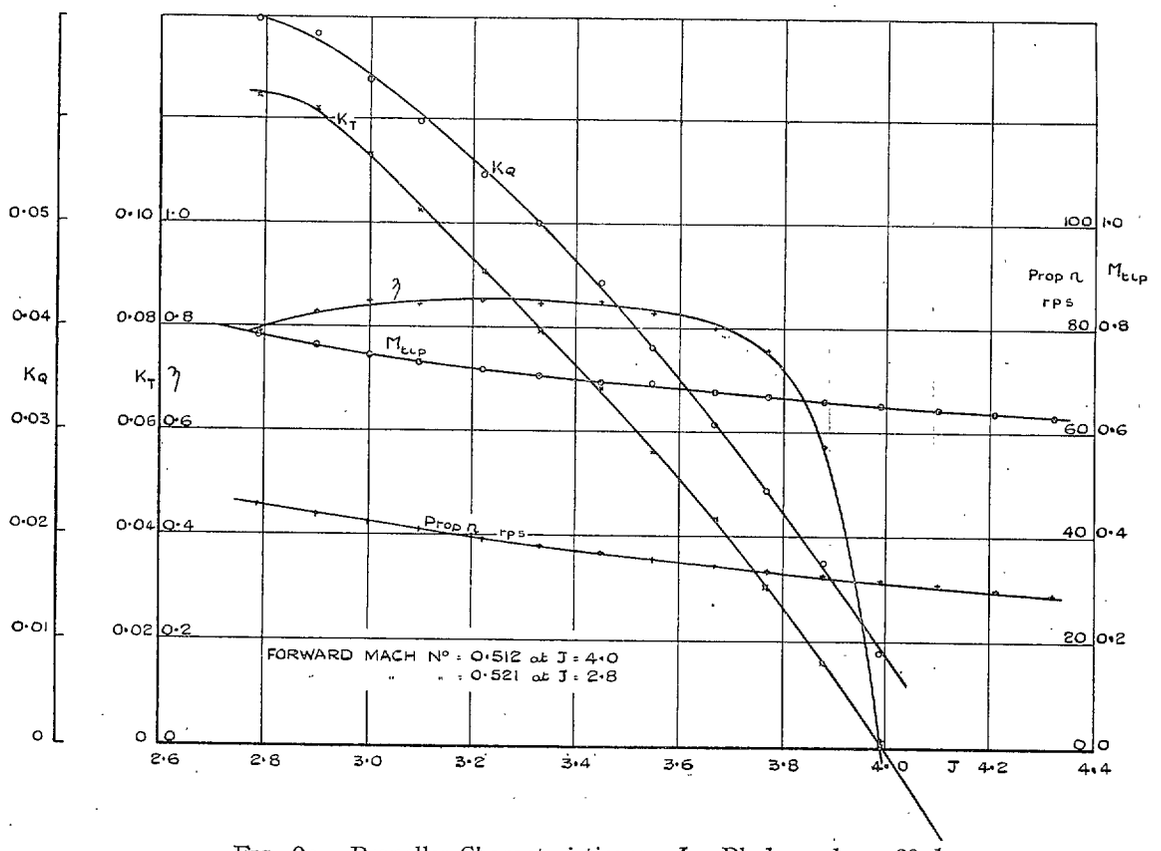

FIG. 9c. Propeller Characteristics vs. J. Blade angle = 60 deg.
Forward Mach number = 0·515.

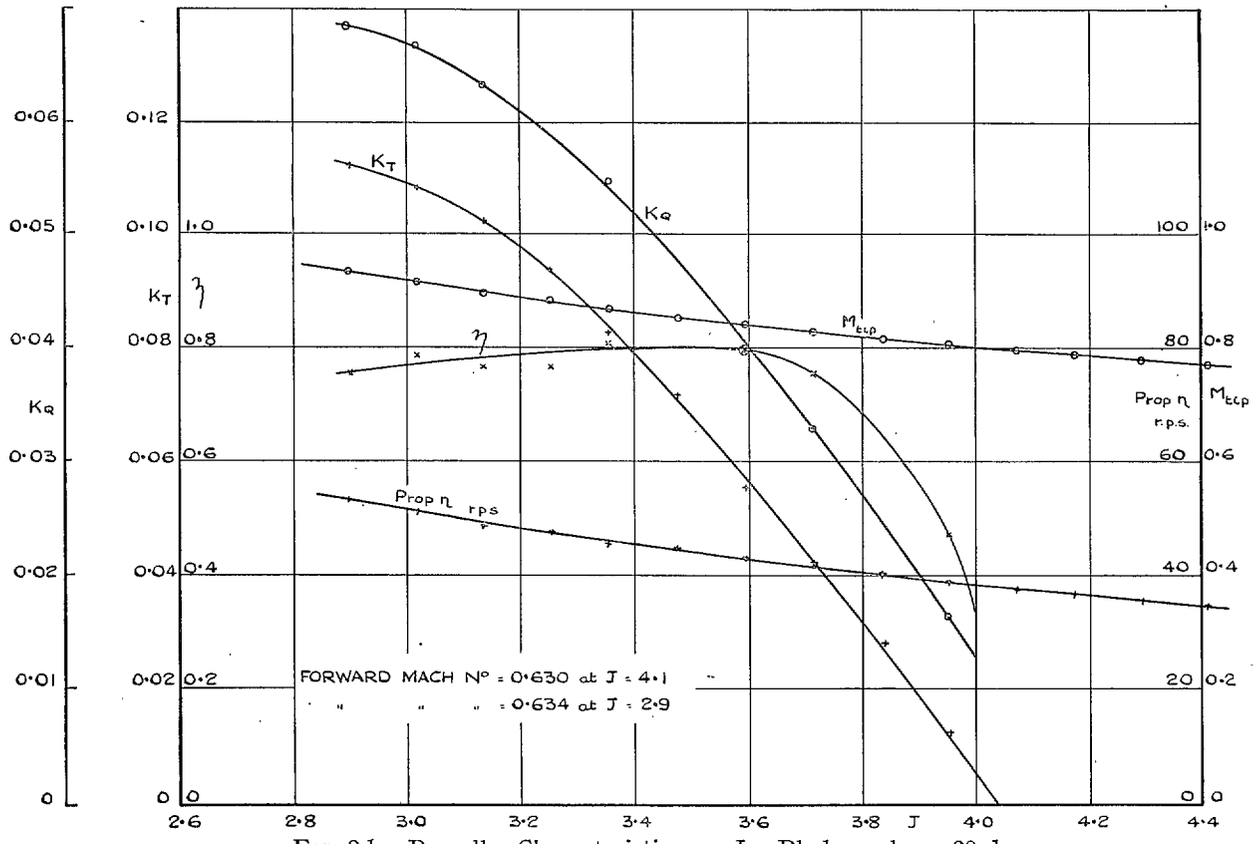

FIG. 9d. Propeller Characteristics vs. J. Blade angle = 60 deg.
Forward Mach number = 0·63.

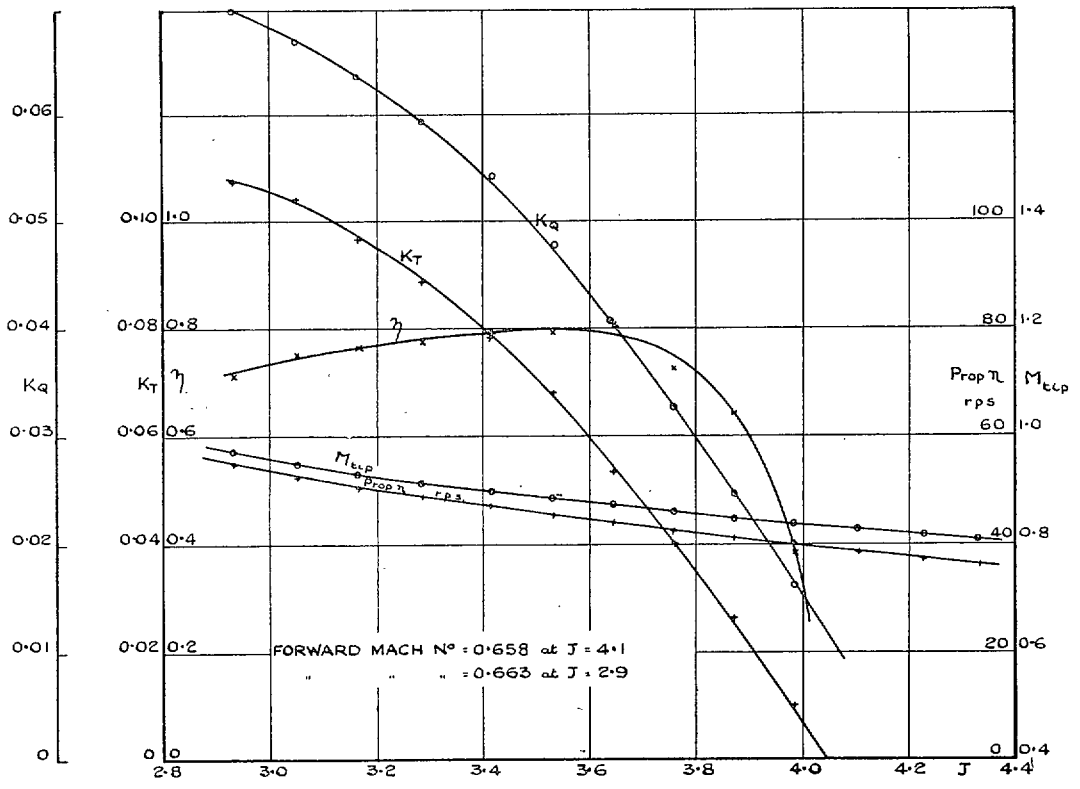

FIG. 9e. Propeller Characteristics vs. J. Blade angle = 60 deg.
Forward Mach number = 0·66.

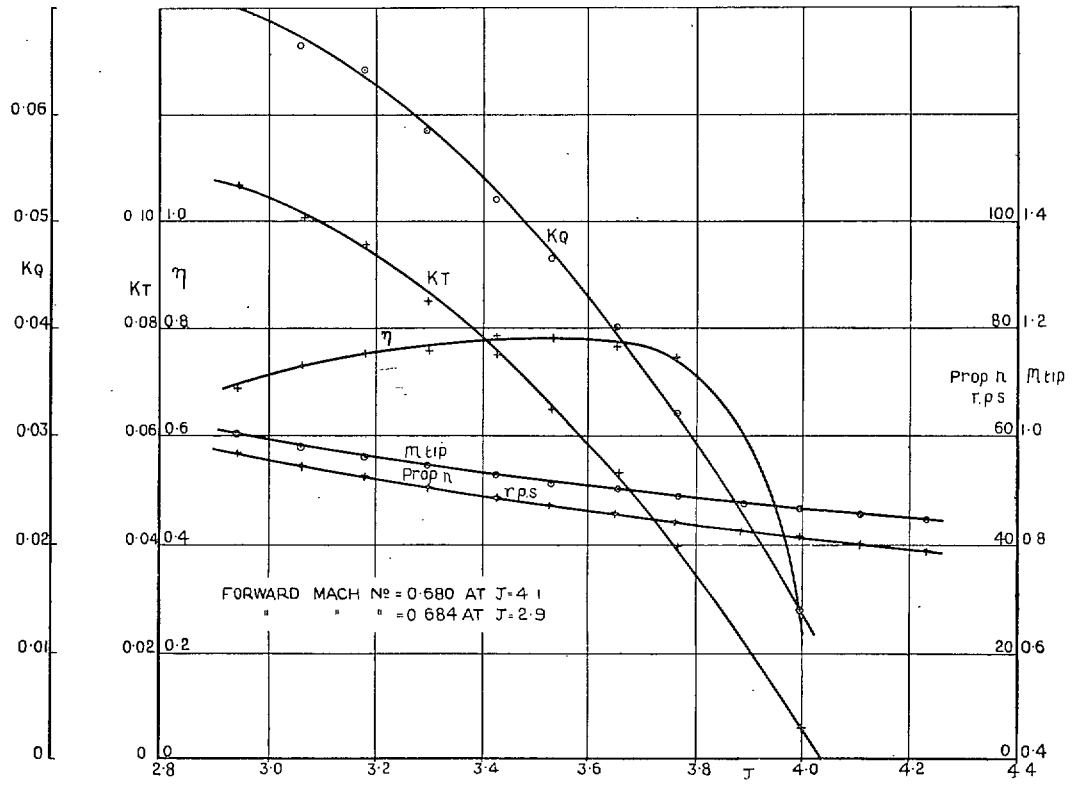

FIG. 9f. Propeller Characteristics vs. J. Blade angle = 60 deg.
Forward Mach number = 0·68.

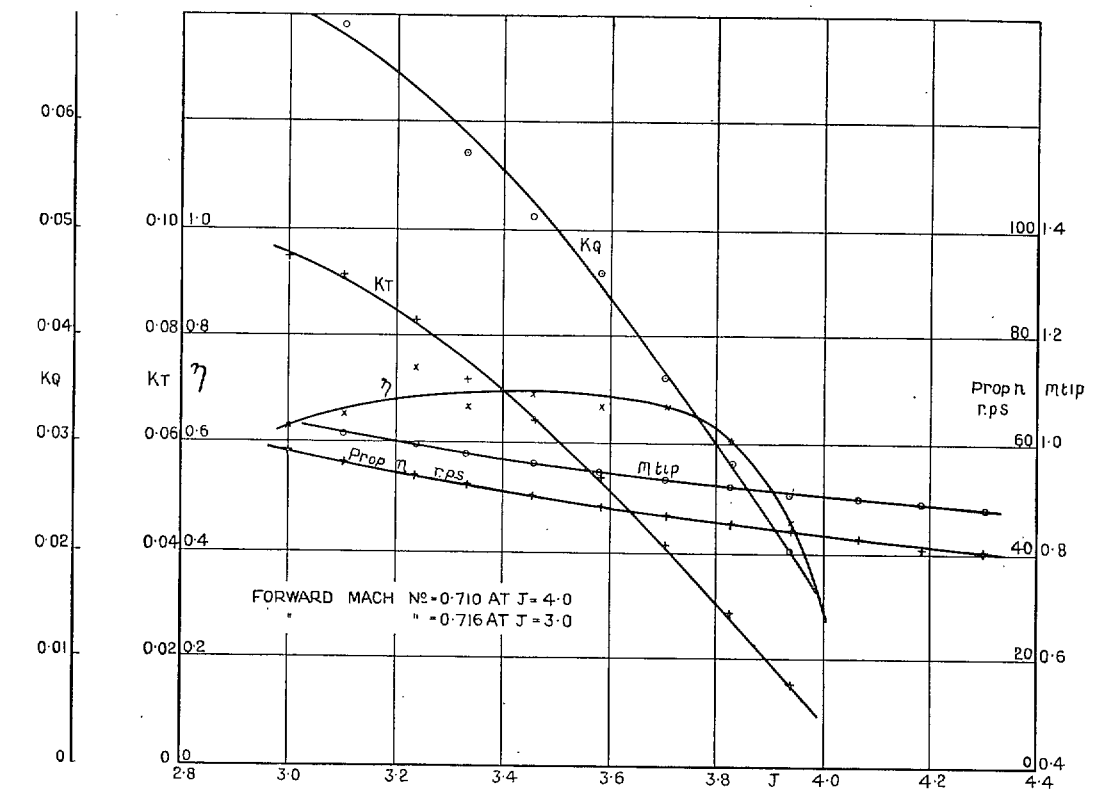

FIG. 9g. Propeller Characteristics vs. J. Blade angle = 60 deg.
Forward Mach number = 0·715.

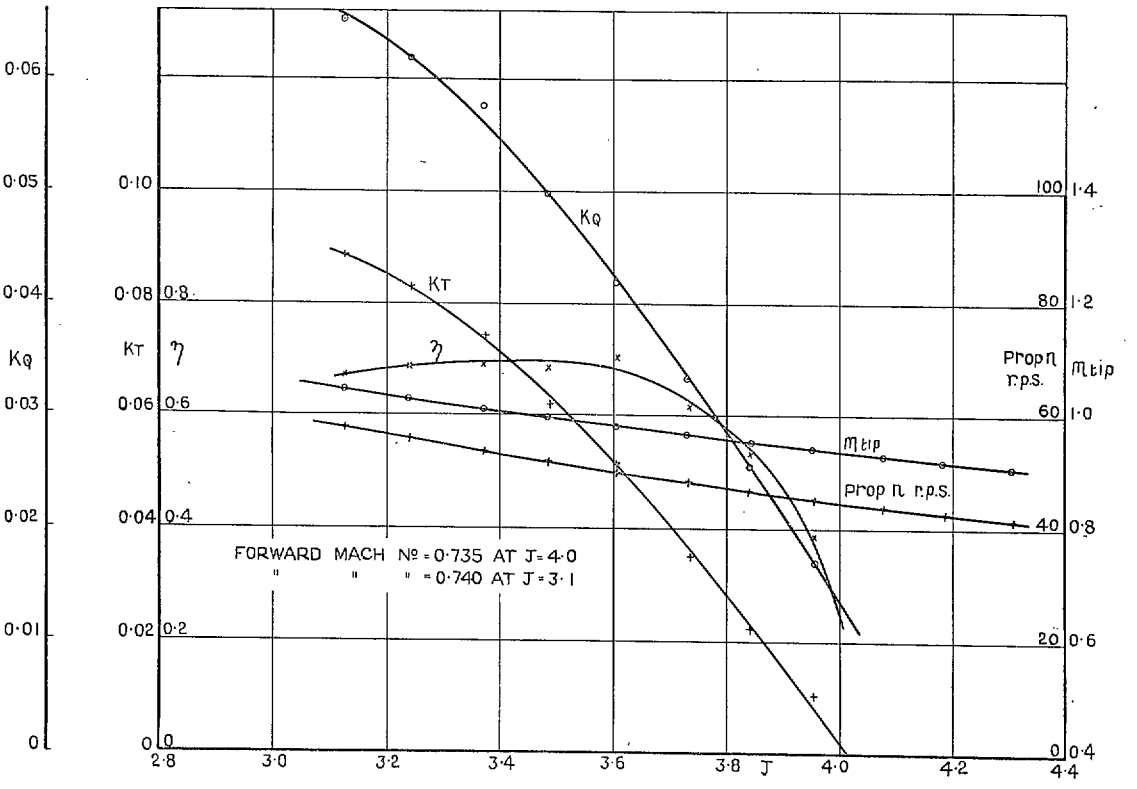

Fig. 9h. Propeller Characteristics vs. J. Blade angle = 60 deg.
Forward Mach number = 0·74.

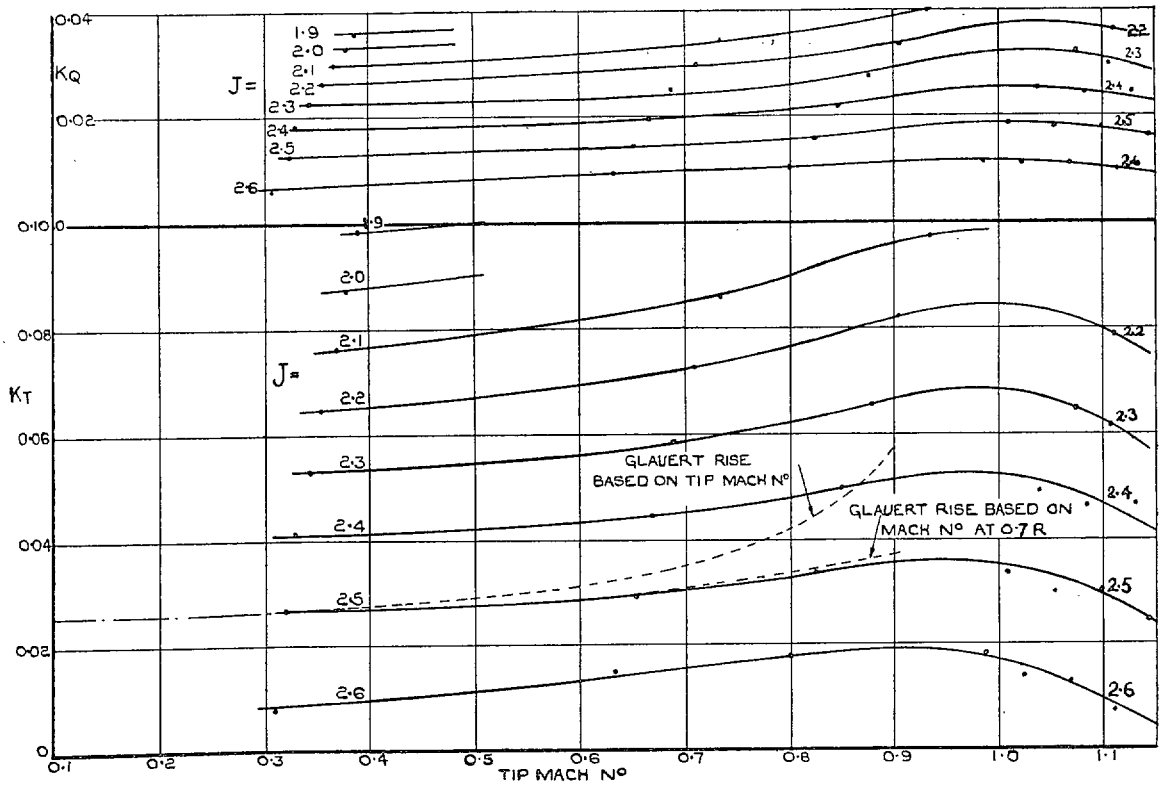

Blade angle $\theta = 60$ deg.

FIG. 10. Variation of K_T and K_Q with Tip Mach number at Constant J.

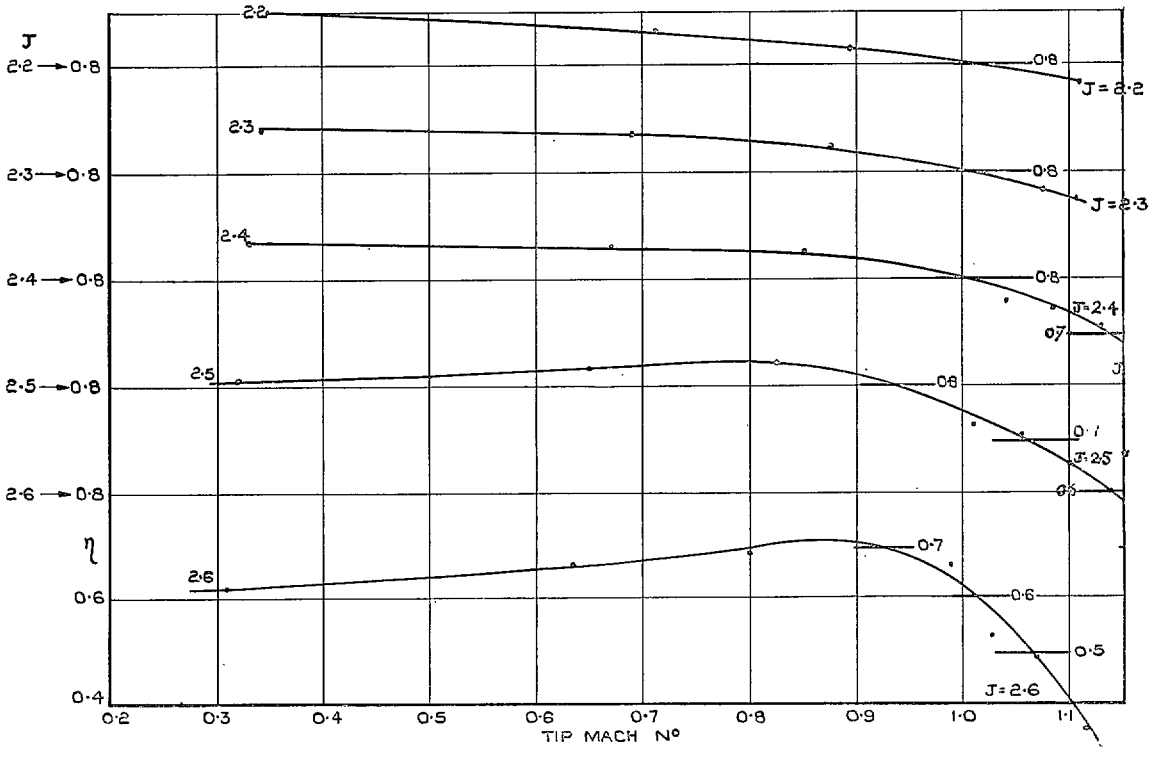

Blade angle $\theta = 50$ deg.

FIG. 11. Variation of Propulsive Efficiency with Tip Mach number at constant J.

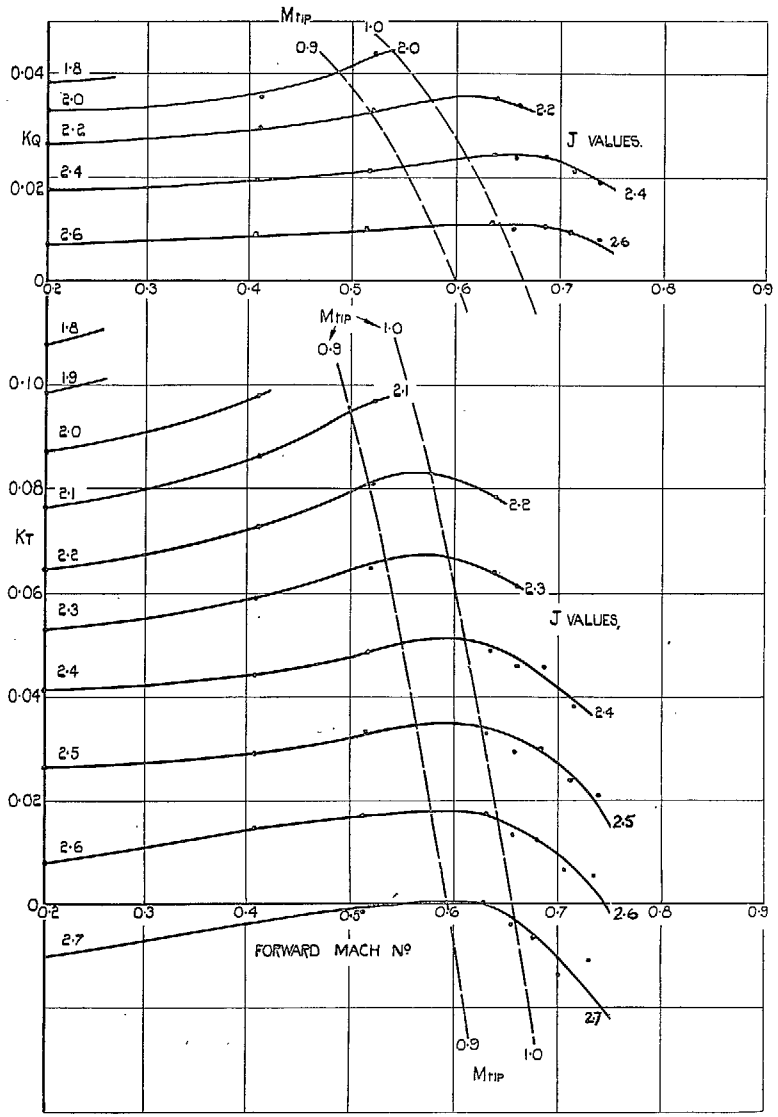

FIG. 12. Blade angle $\theta = 50$ deg.—Variation of Thrust and Torque Coefficients with Forward Mach number at constant J.

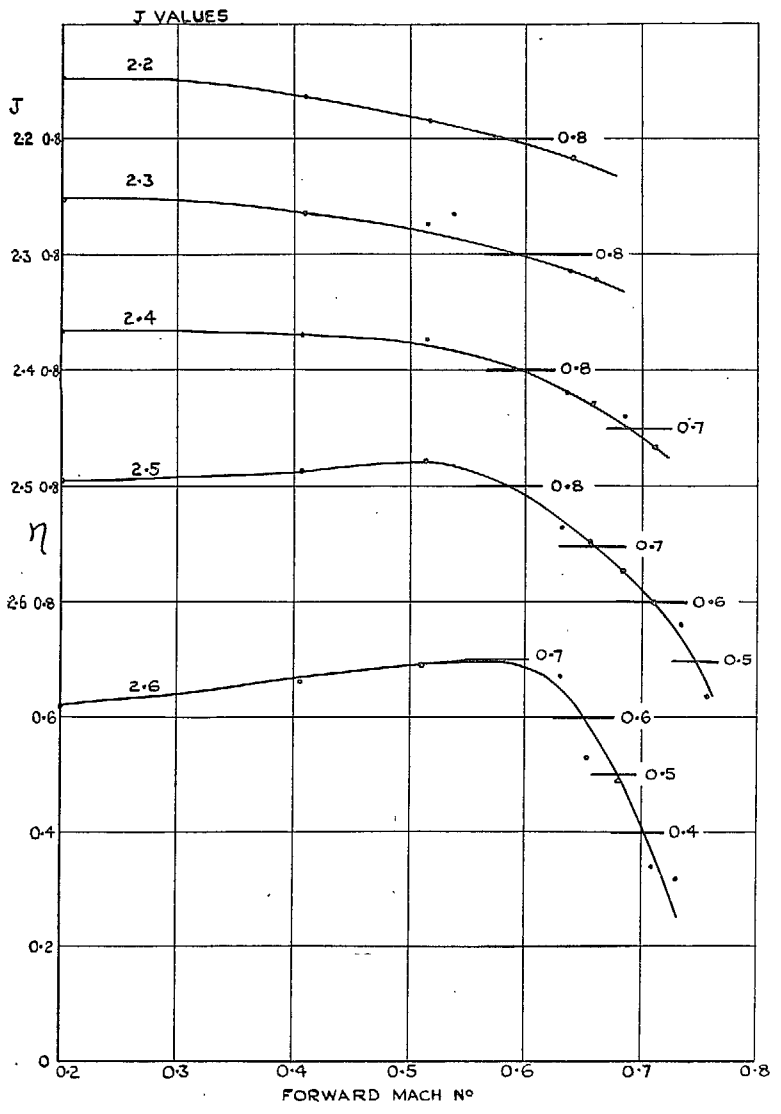

Blade angle $\theta = 50$ deg.

FIG. 13. Variation of Propulsive Efficiency with Forward Mach number at constant J.

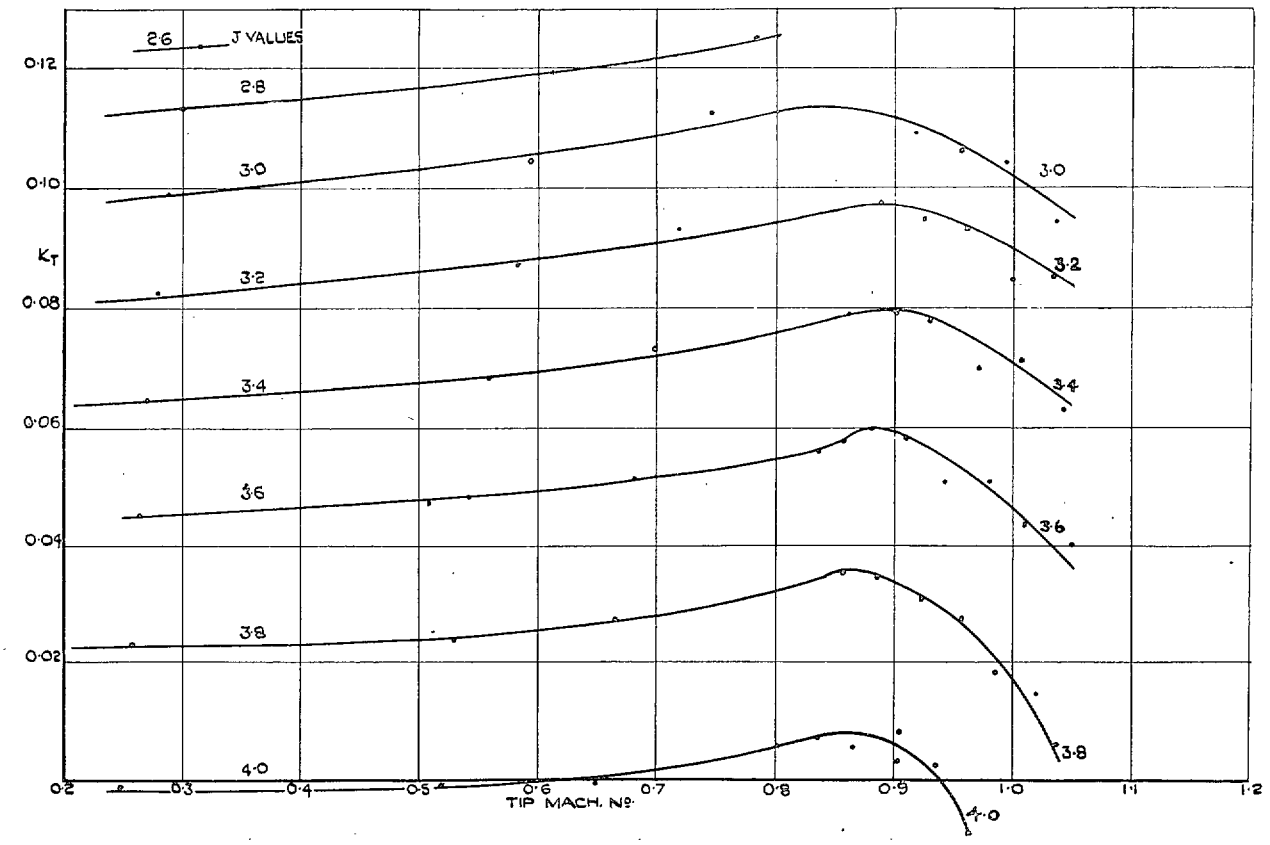

Blade angle $\theta = 60$ deg.

FIG. 14. Variation of K_T with Tip Mach number at constant J.

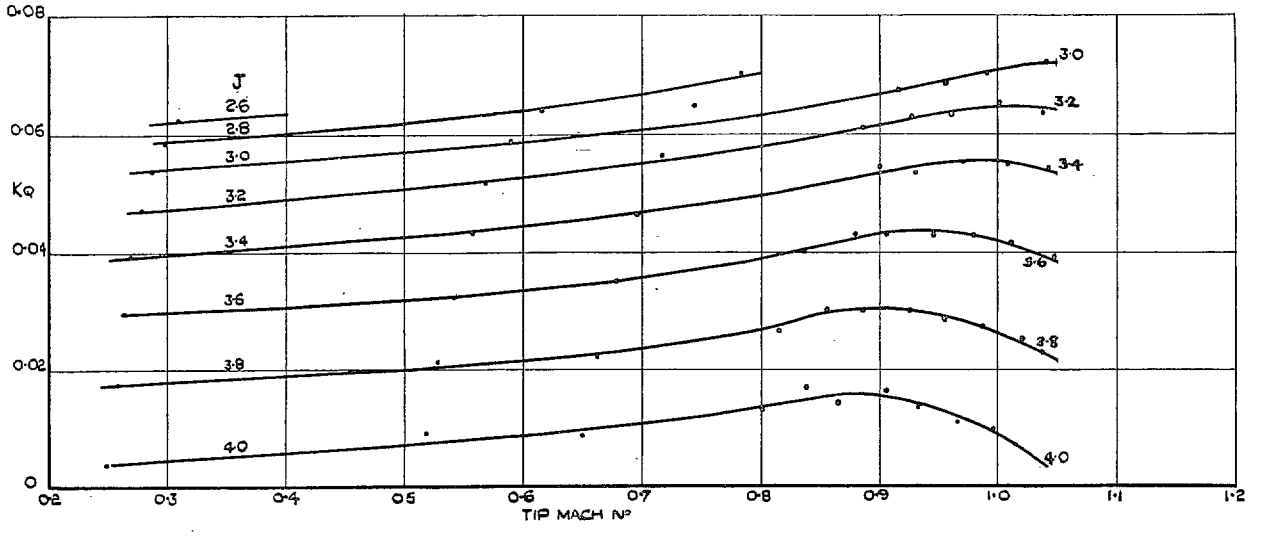

Blade angle $\theta = 60$ deg.

FIG. 15. Variation of K_Q with Tip Mach number at constant J.

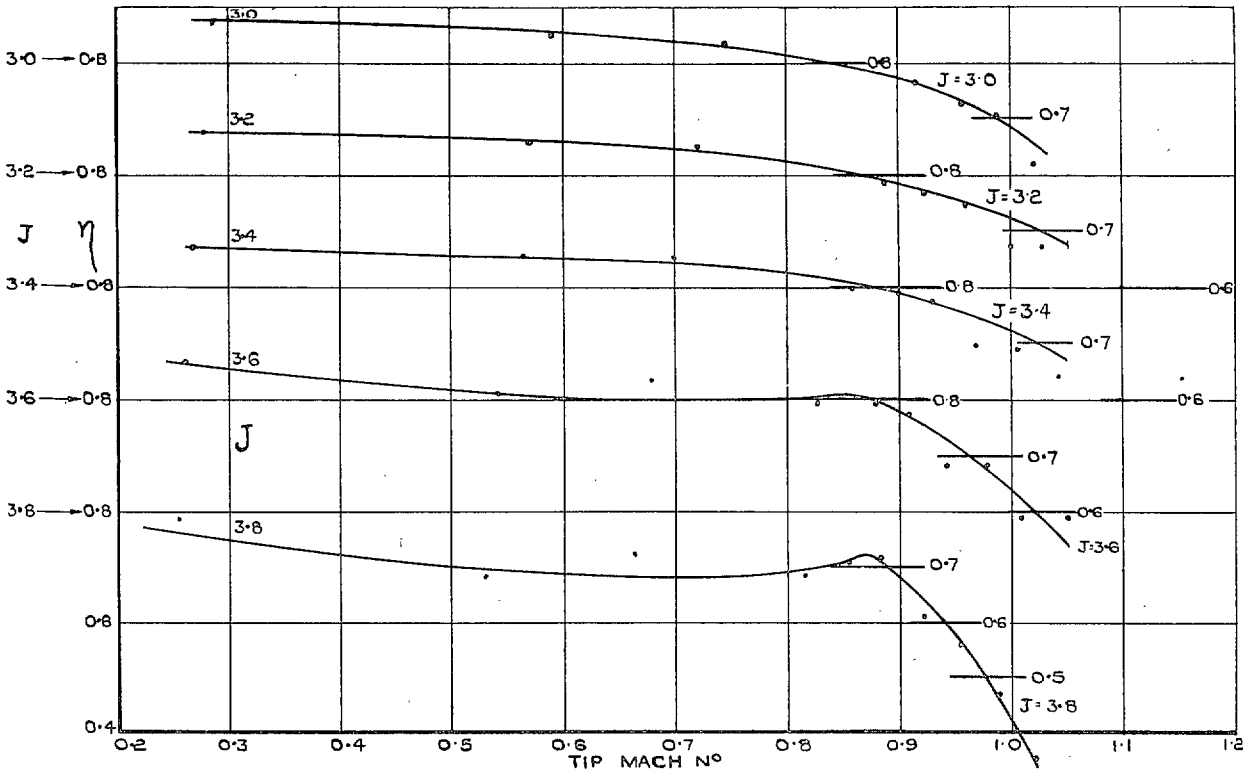

Blade angle $\theta = 60$ deg.

FIG. 16. Variation of Propulsive Efficiency with Tip Mach number at constant J.

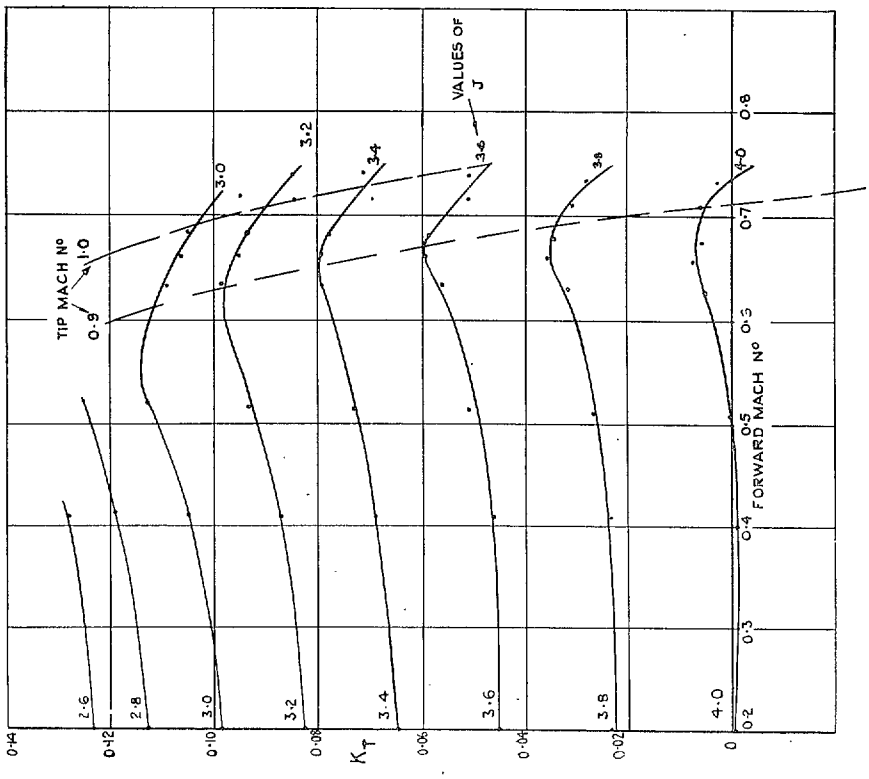

Blade angle $\theta = 60$ deg.

FIG. 17. Variation of Thrust Coefficient with Forward Mach number at constant J.

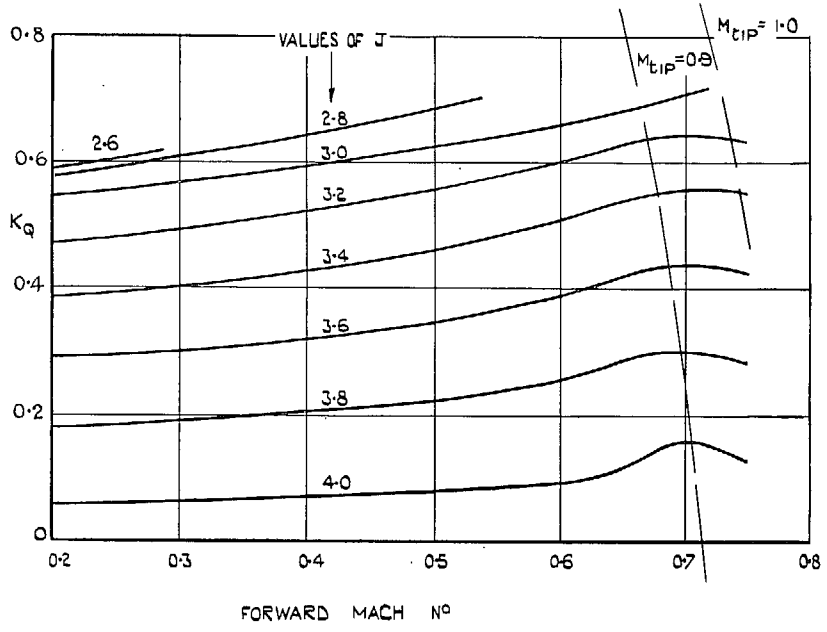

Blade angle $\theta = 60$ deg.

FIG. 18. Variation of Torque Coefficient with Forward Mach number at constant J.

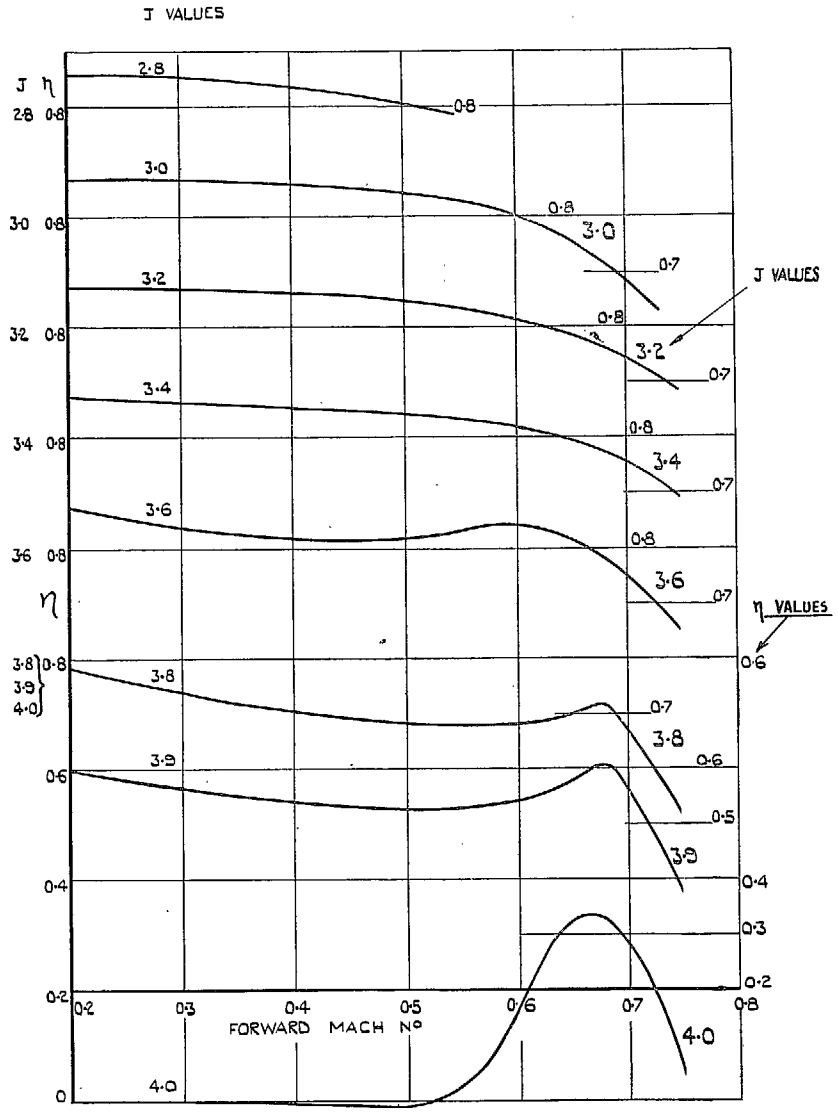

Blade angle $\theta = 60$ deg.

FIG. 19. Variation of Propulsive Efficiency with Forward Mach number at constant J.

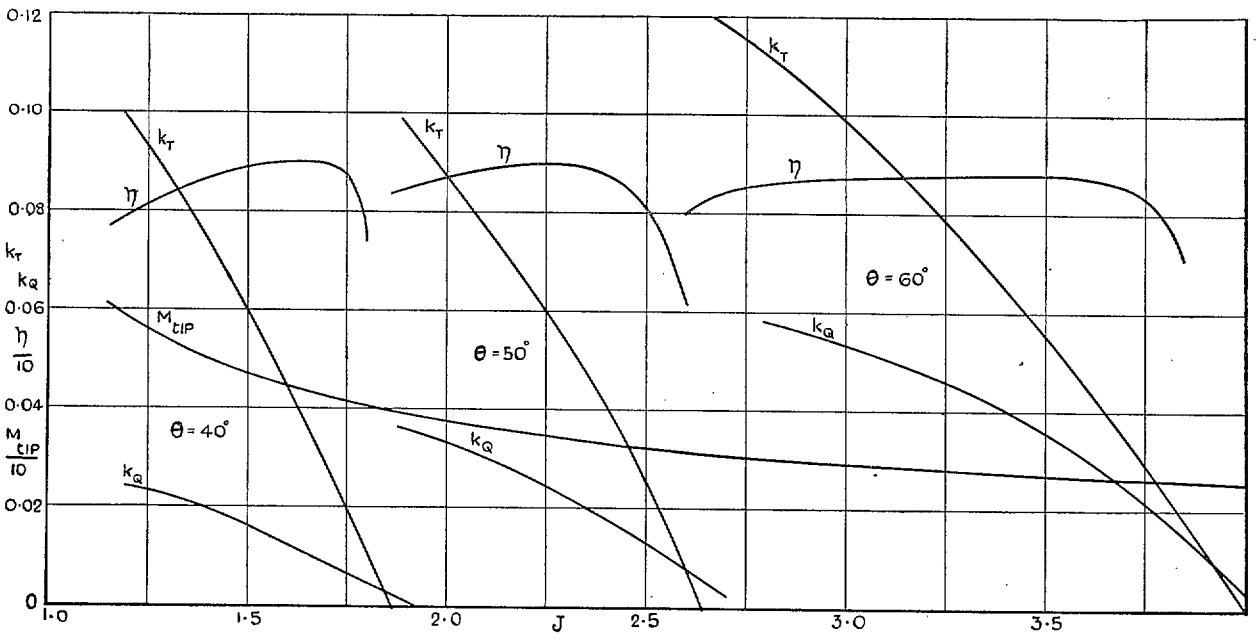

FIG. 20. Propeller Characteristics at Forward Mach number = 0·2.

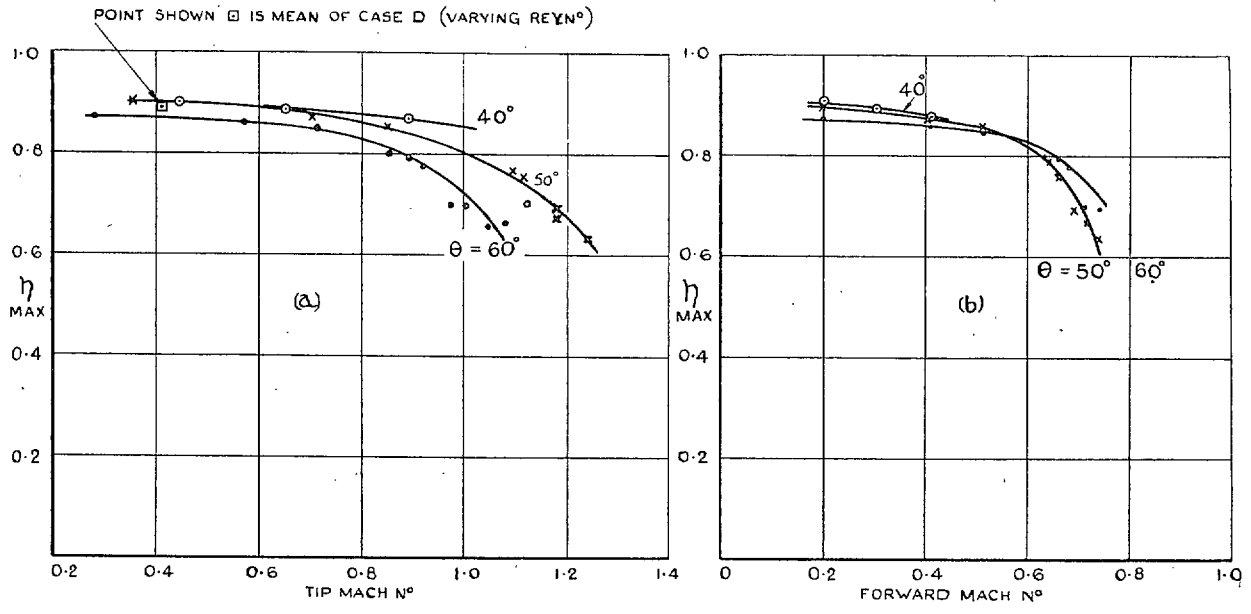

FIG. 21. Variation of Maximum Propulsive Efficiency with Tip and Forward Mach number.

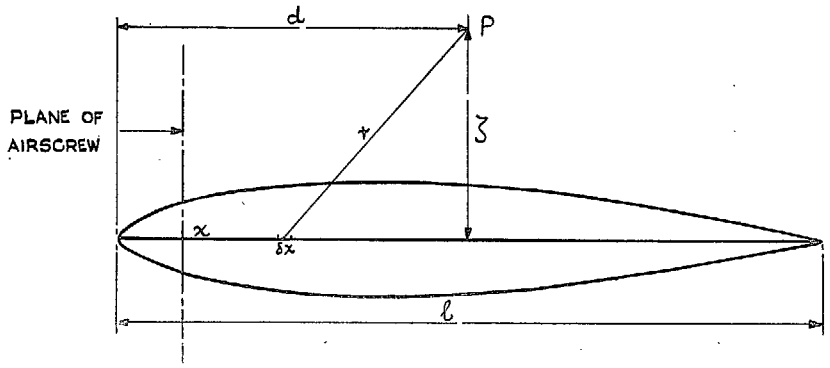

FIG. 22. Co-ordinates of Point in Field of Flow around Motor Body.

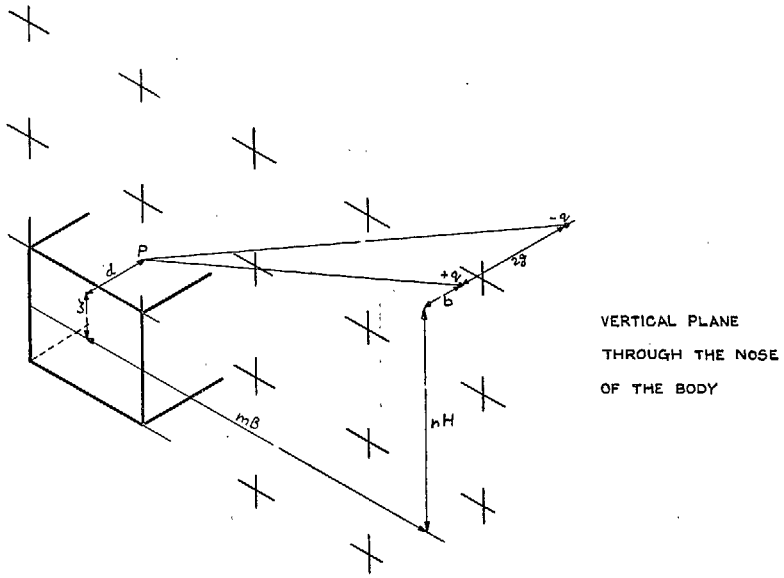

FIG. 24. Image System for Body in High-Speed Tunnel.

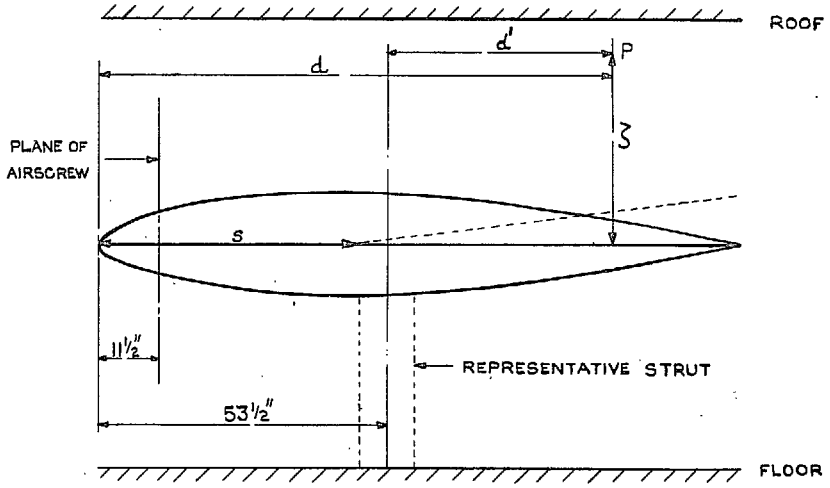

FIG. 23. Representation of Motor and Struts in H.S.T. Working Section.

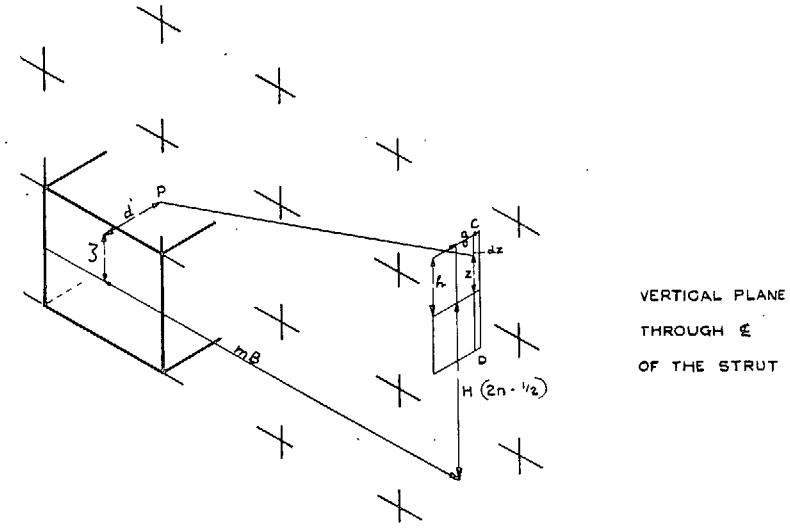

FIG. 25. Image System for Strut in High-Speed Tunnel.

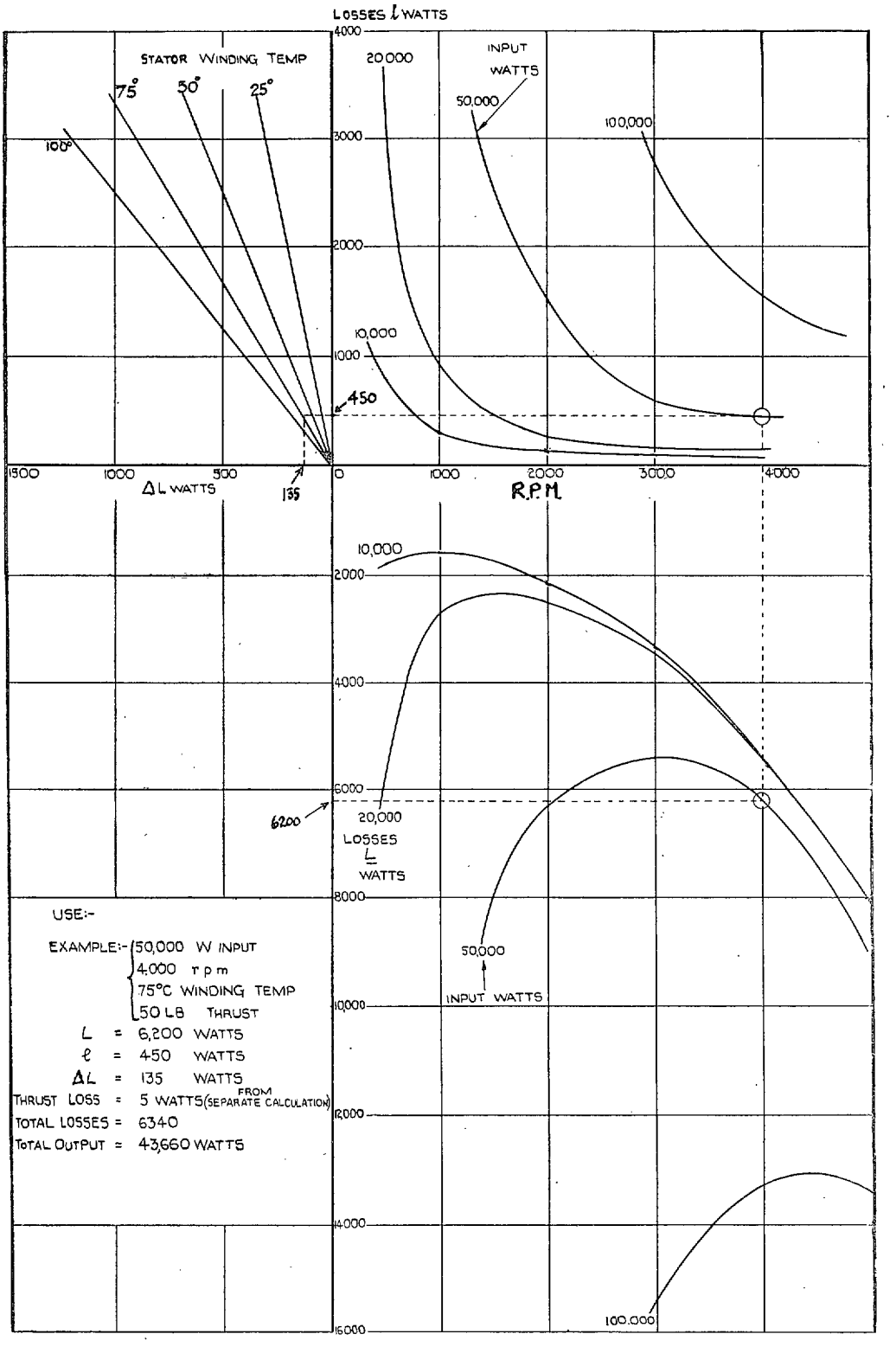

FIG. 26. 200 h.p. Propeller Motor. Motor-loss Determination Chart.

(96128) Wt. 14/806 K.5 6/51 Hw. PRINTED IN GREAT BRITAIN

Publications of the Aeronautical Research Council

ANNUAL TECHNICAL REPORTS OF THE AERONAUTICAL RESEARCH COUNCIL (BOUND VOLUMES)—

1934–35 Vol. I. Aerodynamics. *Out of print.*
Vol. II. Seaplanes, Structures, Engines, Materials, etc. 40*s*. (40*s*. 8*d*.)

1935–36 Vol. I. Aerodynamics. 30*s*. (30*s*. 7*d*.)
Vol. II. Structures, Flutter, Engines, Seaplanes, etc. 30*s*. (30*s*. 7*d*.)

1936 Vol. I. Aerodynamics General, Performance, Airscrews, Flutter and Spinning. 40*s* (40*s*. 9*d*.)
Vol. II. Stability and Control, Structures, Seaplanes, Engines, etc. 50*s*. (50*s*. 10*d*.)

1937 Vol. I. Aerodynamics General, Performance, Airscrews, Flutter and Spinning. 40*s*. (40*s*. 10*d*.)
Vol. II. Stability and Control, Structures, Seaplanes, Engines, etc. 60*s*. (61*s*.)

1938 Vol. I. Aerodynamics General, Performance, Airscrews. 50*s*. (51*s*.)
Vol. II. Stability and Control, Flutter, Structures, Seaplanes, Wind Tunnels, Materials. 30*s*. (30*s*. 9*d*.)

1939 Vol. I. Aerodynamics General, Performance, Airscrews, Engines. 50*s*. (50*s*. 11*d*.)
Vol. II. Stability and Control, Flutter and Vibration, Instruments, Structures, Seaplanes, etc. 63*s*. (64*s*. 2*d*.)

1940 Aero and Hydrodynamics, Aerofoils, Airscrews, Engines, Flutter, Icing, Stability and Control, Structures, and a miscellaneous section. 50*s*. (51*s*.)

Certain other reports proper to the 1940 *volume will subsequently be included in a separate volume.*

ANNUAL REPORTS OF THE AERONAUTICAL RESEARCH COUNCIL—

1933–34	1*s*. 6*d*. (1*s*. 8*d*.)
1934–35	1*s*. 6*d*. (1*s*. 8*d*.)
April 1, 1935 to December 31, 1936.	4*s*. (4*s*. 4*d*.)
1937	2*s*. (2*s*. 2*d*.)
1938	1*s*. 6*d*. (1*s*. 8*d*.)
1939–48	3*s*. (3*s*. 2*d*.)

INDEX TO ALL REPORTS AND MEMORANDA PUBLISHED IN THE ANNUAL TECHNICAL REPORTS, AND SEPARATELY—

April, 1950 — R. & M. No. 2600. 2*s*. 6*d*. (2*s*. 7½*d*.)

INDEXES TO THE TECHNICAL REPORTS OF THE AERONAUTICAL RESEARCH COUNCIL—

December 1, 1936 — June 30, 1939.	R. & M. No. 1850.	1*s*. 3*d*. (1*s*. 4½*d*.)
July 1, 1939 — June 30, 1945.	R. & M. No. 1950.	1*s*. (1*s*. 1½*d*.)
July 1, 1945 — June 30, 1946.	R. & M. No. 2050.	1*s*. (1*s*. 1½*d*.)
July 1, 1946 — December 31, 1946.	R. & M. No. 2150.	1*s*. 3*d*. (1*s*. 4½*d*.)
January 1, 1947 — June 30, 1947.	R. & M. No. 2250.	1*s*. 3*d*. (1*s*. 4½*d*.)

Prices in brackets include postage.

Obtainable from

HIS MAJESTY'S STATIONERY OFFICE

York House, Kingsway, LONDON, W.C.2 — 429 Oxford Street, LONDON, W.1
P.O. Box 569, LONDON, S.E.1
13a Castle Street, EDINBURGH, 2 — 1 St. Andrew's Crescent, CARDIFF
39 King Street, MANCHESTER, 2 — Tower Lane, BRISTOL, 1
2 Edmund Street, BIRMINGHAM, 3 — 80 Chichester Street, BELFAST

or through any bookseller.